JOURNAL OF GEOPHYSICAL RESEARCH, VOL. 112, D22301, doi:10.1029/2007JD008459, 2007

Global budget of CO, 1988–1997: Source estimates and validation with a global model

B. N. Duncan,[1,2,3] J. A. Logan,[1] I. Bey,[1,4] I. A. Megretskaia,[1] R. M. Yantosca,[1] P. C. Novelli,[5] N. B. Jones,[6,7] and C. P. Rinsland[8]

Received 25 January 2007; revised 25 May 2007; accepted 7 August 2007; published 17 November 2007.

[1] We present a model study of carbon monoxide for 1988–1997 using the GEOS-Chem 3-D model driven by assimilated meteorological data, with time-varying emissions from biomass burning and from fossil fuel and industry, overhead ozone columns, and methane. The hydroxyl radical is calculated interactively using a chemical parameterization to capture chemical feedbacks. We document the inventory for fossil fuels/industry and discuss major uncertainties and the causes of differences with other inventories that give significantly lower emissions. We find that emissions hardly change from 1988 to 1997, as increases in Asia are offset by decreases elsewhere. The model reproduces the 20% decrease in CO at high northern latitudes and the 10% decrease in the North Pacific, caused primarily by the decrease in European emissions. The model compares well with observations at sites impacted by fossil fuel emissions from North America, Europe, and east Asia suggesting that the emissions from this source are reliable to 25%, and we argue that bottom-up emission estimates are likely to be too low rather than too high. The model is too low at the seasonal maximum in spring in the southern tropics, except for locations in the Atlantic Ocean. This problem may be caused by an overestimate of the frequency of tropical deep convection, a common problem in models that use assimilated meteorological data. We argue that the yield of CO from methane oxidation is near unity, contrary to some other studies, based on removal rates of intermediate species.

Citation: Duncan, B. N., J. A. Logan, I. Bey, I. A. Megretskaia, R. M. Yantosca, P. C. Novelli, N. B. Jones, and C. P. Rinsland (2007), Global budget of CO, 1988–1997: Source estimates and validation with a global model, *J. Geophys. Res.*, *112*, D22301, doi:10.1029/2007JD008459.

1. Introduction

[2] Carbon monoxide plays important roles in atmospheric chemistry. Reaction with carbon monoxide (CO) provides the dominant sink for the hydroxyl radical (OH), the main tropospheric oxidant, and oxidation of CO provides a source or a sink for ozone, depending on levels of nitrogen oxides (NO_x) [e.g., *Levy*, 1971; *Crutzen*, 1973; *Logan et al.*, 1981]. Changes in emissions of CO have the potential to influence climate by affecting methane and other radiatively important gases that are removed by OH, and by affecting tropospheric ozone itself [e.g., *Daniel and Solomon*, 1988; *Mickley et al.*, 1999].

[3] Carbon monoxide increased in the Northern Hemisphere (NH) from the 1950s until the 1980s and decreased from the late 1980s until mid-1997 [*Zander et al.*, 1989; *Khalil and Rasmussen*, 1994; *Novelli et al.*, 1994, 1998, 2003]. There were large increases in CO in the NH associated with anomalously large forest fires in 1998, 2002, and 2003; however, levels in 2000 and 2001 were similar to those in 1997 [*Novelli et al.*, 2003; *Yurganov et al.*, 2004, 2005]. Part of the downward trend in CO in the early 1990s has been attributed to the effects of the Mount Pinatubo eruption in June 1991, when ozone levels in the lower stratosphere were reduced and tropospheric OH was enhanced [*Bekki et al.*, 1994; *Novelli et al.*, 1994; *Dlugokencky et al.*, 1996].

[4] The temporal behavior of CO is best documented by surface measurements from the NOAA Earth System Research Laboratory, Global Monitoring Division (GMD) that started in 1988 [*Novelli et al.*, 1994, 1998, 2003], and by column measurements at a few locations [e.g., *Mahieu et*

[1]School of Engineering and Applied Sciences, Harvard University, Cambridge, Massachusetts, USA.
[2]Now at Goddard Earth Sciences and Technology Center, University of Maryland, Baltimore County, Baltimore, Maryland, USA.
[3]Also at NASA Goddard Space Flight Center, Greenbelt, Maryland, USA.

0148-0227/07/2007JD008459$09.00

[4]Now at Laboratoire de Modélisation de Chimie Atmosphérique, École Polytechnique Fédérale de Lausanne, Lausanne, Switzerland.
[5]Global Monitoring Division, Earth System Research Laboratory, NOAA, Boulder, Colorado, USA.
[6]National Institute of Water and Atmospheric Research, Lauder, New Zealand.
[7]Now at Department of Chemistry, University of Wollongong, Wollongong, New South Wales, Australia.
[8]NASA Langley Research Center, Hampton, Virginia, USA.

Table 1. Budget for CO Sources in the GEOS-Chem Model With Comparison to the Budget of *Holloway et al.* [2000][a]

	This Work			
	Direct Emission[b]	Photochemical Oxidation[b,c]	Sum	*Holloway et al.* [2000]: Sum
Combustion				
Fossil fuels	391–411	72–76	464–487	300[d]
Biofuels	159	30	189	162[d,e]
Biomass burning	406–516	45–57	451–573	586[d,e]
Biogenic NMHC				
Isoprene	–	170–184	170–184	648
Monoterpenes	–	68–71	68–71	24
Methanol	–	95–103	95–103	–
Acetone	–	21	21	–
CH_4 oxidation	–	778–861	778–861	760
Ocean	–	–	–	–
Sum	956–1086	1279–1403	2236–2489	2491

[a]Unit is Tg/a.
[b]The range given represents the range of CO production rates for the entire model simulation time period (1988–1997).
[c]Photochemical oxidation of NMHC or CH_4.
[d]Does not include CO produced from the photochemical oxidation of anthropogenic NMHC.
[e]Sum of CO from biomass burning categories of forests, savannas, agricultural residues and biofuel categories of fuelwood, domestic crop residues, and dried animal wastes [*Galanter et al.*, 2000].

al., 1997; *Zhao et al.*, 1997; *Rinsland et al.*, 1998, 1999, 2000; *Zhao et al.*, 2000; *Yurganov et al.*, 2004]. In this paper we use these data to test current understanding of the CO budget. In a companion paper, we investigate the causes of trends and interannual variability (IAV) of CO from 1988 to 1997 (B. N. Duncan and J. A. Logan, Model analysis of the factors regulating the trends of carbon monoxide, 1988–1997, manuscript in preparation, 2007, hereinafter referred to as Duncan and Logan, manuscript in preparation, 2007).

[5] We selected the period 1988–1997 for analysis for several reasons. There were major changes in the distributions of anthropogenic emissions because of the economic contraction of the former Soviet Union and the rapid industrialization of east Asia [*U.S. Environmental Protection Agency* (*U.S. EPA*), 1997; *European Monitoring Environmental Programme* (*EMEP*), 1997; *Marland et al.*, 1999; *United Nations*, 1998]. Stratospheric O_3 columns decreased from about 1980 until the mid-1990s and reached record lows after the eruption of Mount Pinatubo in June 1991 [*World Meteorological Organization* (*WMO*), 1999]. Changes in the O_3 column affect the tropospheric distributions of trace gases that react with OH, including CO [*Bekki et al.*, 1994; *Novelli et al.*, 1994; *Dlugokencky et al.*, 1996, 1998]. Several large tropical biomass burning events occurred during 1988–1997, including major fires in Indonesia in 1997 [*Levine*, 1999; *Duncan et al.*, 2003b], but there were not large perturbations to CO from major boreal fires as in later years [*Yurganov et al.*, 2004, 2005].

[6] Fossil fuel combustion provides the dominant source of CO at northern midlatitudes, while the main sources in the tropics are oxidation of CH_4 and biogenic nonmethane hydrocarbons (NMHC), and biomass burning [e.g., *Logan et al.*, 1981; *Holloway et al.*, 2000]. There are significant uncertainties in the magnitude and spatial distribution of most sources. An intercomparison of 3-D chemical transport models (CTMs) a few years ago showed that a wide range of emission rates for CO were being used, and that many of the models' results did not agree with observations at the GMD sites [*Kanakidou et al.*, 1999]. A new intercomparison of 26 CTMs also showed a wide range of simulated CO distributions, even though the models all used the same emissions for fuel combustion, industry, and biomass burning [*Shindell et al.*, 2006]; the differences resulted in part from the OH fields in the models. Here we summarize results from recent CTM studies that focused on constraining the CO budget and on explaining trends and IAV. Emissions used in these studies are given in Tables 1 and 2.

[7] *Holloway et al.* [2000] performed a detailed study using a CTM driven by winds from a general circulation model, with specified OH distributions. They found that CH_4 oxidation provides a uniform CO background of about 25 ppbv everywhere (as did *Granier et al.* [2000]). Their model underestimated CO in spring at sites in the northern extratropics, which they attributed to an underestimate of their emissions from fossil fuel/industry, ~300 Tg/a. Several studies using inverse modeling techniques, with similar magnitudes for the fossil fuel/industrial source as their prior, also found that this source appears to be underestimated [*Bergamaschi et al.*, 2000a, 2000b; *Kasibhatla et al.*, 2002; *Pétron et al.*, 2002, 2004; *Arellano et al.*, 2004, 2006; *Müller and Stavrakou*, 2005]. These studies relied on the EDGAR inventory [*Olivier et al.*, 1996] for their prior, and their inversions give a range of 642–870 Tg CO/a for direct emissions from fuel combustion and industry (Table 2). Most of these global inversion analyses found that fossil and biofuel sources from Asia are significantly underestimated by the EDGAR inventory, although their results differ in detail. The new intercomparison study of Shindell et al., which was based on the EDGAR inventory, found that all forward models underestimated CO in the northern extratropics. Analyses of the aircraft data downwind of Asia imply that emissions of CO from China are much too low in the *Streets et al.* [2003] inventory [*Carmichael et al.*, 2003; *Palmer et al.*, 2003; *Allen et al.*, 2004]. A new bottom-up inventory, motivated by these studies, gives emissions for China that are 36% higher than the earlier study [*Streets et al.*, 2006].

Table 2. CO Sources Derived From Inversion Analyses[a]

	Bergamaschi et al. [2000a][b]	*Pétron et al.* [2002][c]	*Pétron et al.* [2004]	*Müller and Stavrakou* [2005][d]	*Kasibhatla et al.* [2002][e]	*Arellano et al.* [2004]	*Arellano et al.* [2006]
Model	TM2	IMAGES	MOZART	IMAGES	GEOS-Chem	GEOS-Chem	GEOS-Chem
Data constraint	GMD	GMD	MOPITT[f]	GMD	GMD	MOPITT[g]	MOPITT[g]
Year of data	1993–1995	1990–1996	Apr 2000 to Mar 2001	1997	1993–1995	2000	Apr 2000 to Apr 2001
Type of source for FF, BF, BB[h]	DE	DE	DE	DE	DE+HCOx	DE+HCOx	DE+HCOx
Fossil fuel (FF), industrial		309	365				
Biofuel (BF)		561[i]	318				
FF + BF	642	870	683	760	857 (768)	844–923	841
Anthropogenic HC oxidation	166						
Biomass burning (BB)	722	606	408	359	561 (467)	508–579	501
Biogenic, soils		167		142		–	–
Oxidation of biogenic HCs	507				477 (362)	175–209	394
Oxidation of all HCs				774			
Ocean	23	20		23		–	–
CH_4 oxidation	830			870	949 (709)	767	820
Total surface emission	1364	1663, 1528–1694	1091	1261	1418 (1235)	1352–1502	1342
Total oxidation source	1503	1461–1536	1650	1644			
Total source	2891	2960–3067	2741	2928	2846 (2306)	2294–2478	2556
OH sink	2597		2630			~2388	2618
CO deposition	294			203	–	–	–
MCF tropospheric lifetime, a	5.1	4.41			5.1 (6.4)	6.6	6.4

[a]Note that not all budget terms were available for each study.
[b]S2 base scenario, CH_4 source was fixed in inversion.
[c]Results from second iteration.
[d]Case A, inverting for CO only.
[e]Values in parentheses are for the OH field reduced by 20%.
[f]MOPITT data at 700 hPa used in the inversion.
[g]MOPITT column data used in the inversion.
[h]Different studies give either the source of CO or the source of CO plus the CO derived from coemitted NMHC for the fossil fuel, biofuel, and biomass burning sources of CO. DE, direct emission; DE + HCOx, direct emission plus CO from NMHC oxidation.
[i]Includes agricultural waste burning.

[8] *Holloway et al.* [2000] found reasonable agreement between their model and surface measurements in the tropics. However, they invoke a high CO source from isoprene oxidation (~650 Tg CO/a), assuming that most of the carbon is oxidized to CO in a low-NO_x environment. Most other studies assume a lower yield of CO based on laboratory measurements [e.g., *Paulson and Seinfeld*, 1992; *Miyoshi et al.*, 1994; *Granier et al.*, 2000]. *Bergamaschi et al.* [2000a] and *Pétron et al.* [2002] used a much higher CO source from biomass burning than is given by bottom-up inventories of *Olivier et al.* [2001] and *Duncan et al.* [2003a], and their inversion results imply a larger biomass burning source (606–722 Tg CO/a) than those from other inversions (359–580 Tg CO/a) as shown in Table 2. Pétron et al. and Kasibhatla et al. found that the biomass burning source is not well constrained in their inversions using GMD data.

[9] *Allen et al.* [1996a] investigated the influence of IAV in transport on CO for 1988–1993, using assimilated meteorological fields, but with the same emissions and OH fields for the entire period. They found that transport-induced variability explained over 80% of the variances and short-term trends at sites in (or near) the north Atlantic influenced by continental pollution, but much less of the variances at remote sites.

[10] *Karlsdóttir et al.* [2000] used a CTM with interactive chemistry to study the effects of trends in fossil fuel emissions on CO for 1980–1996, using 1 a of meteorological fields. Their model gave a small upward trend in OH, but did not capture the observed downward trend in CO in the first half of the 1990s in the NH.

[11] In this paper and its companion (Duncan and Logan, manuscript in preparation, 2007), we investigate the uncertainties in the budget of CO, and the causes of its trends and IAV from 1988 to 1997, using the GEOS-Chem 3-D model driven by assimilated meteorological fields from Goddard Earth Observing System Global Modeling and Assimilation Office (GEOS GMAO). Unlike previous studies, we allow for IAV in sources from fossil fuel use and from biomass burning, and we allow for feedback between CO and OH. We also account for IAV in the overhead ozone column and for the observed trend in CH_4. We first document the emissions used in the model and discuss their uncertainties. We then discuss the model's ability to reproduce observations, including trends and IAV, with a focus on (1) understanding which sources contribute to the observed distributions in various regions and (2) providing constraints on the emission inventories. We conduct simulations to demonstrate the sensitivity of CO to OH and to emissions.

[12] In our companion paper, we explore the causes of trends and IAV of CO from 1988 to 1997 (Duncan and Logan, manuscript in preparation, 2007). Using a series of sensitivity simulations, we deconvolve the impacts

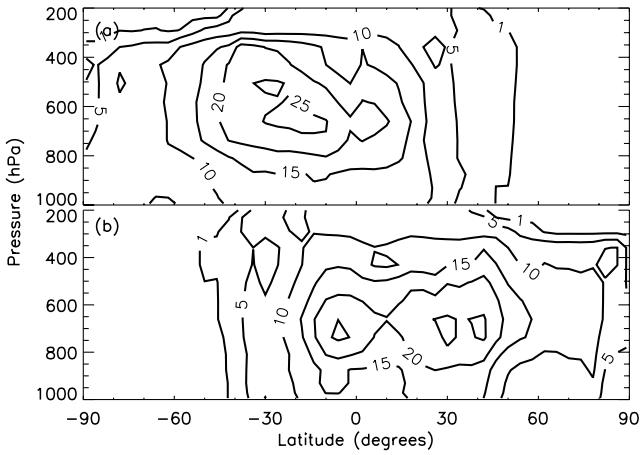

Figure 1. Zonal mean OH (10^5 molecules cm^{-3}) simulated by the parameterization of OH for (a) January and (b) July 1994.

on CO of IAV and trends in biomass burning and fossil fuel emissions, the overhead ozone column, methane, and meteorology. We also investigate the impact of these causal factors on OH.

[13] The model is described in section 2. In section 3, we describe sources of CO used in the simulations, while observations used for model evaluation are described in section 4. We discuss the contributions from different sources to the total burden of CO in section 5.1. We discuss the major features in CO over the 10-a simulation period and evaluate the model using observations in sections 5.2–5.4. The sensitivity of CO to changes in OH and emission sources is explored in section 6. A discussion and conclusions are given in section 7.

2. Model Framework

[14] The GEOS-Chem 3-D model was first described by *Bey et al.* [2001a]. Here we describe a new CO-only version of the model that includes an online OH parameterization [*Duncan et al.*, 2000]. We also document in detail the sources of CO, including those not included in the early version of GEOS-Chem (CO from oxidation of monoterpenes, methanol, and NMHC emitted by biofuel consumption).

[15] The model is driven by assimilated meteorological data from the GEOS GMAO [*Schubert et al.*, 1993, 1995; *Takacs et al.*, 1994; *Takacs*, 1995]. Two versions of GEOS products were used in this study: GEOS-1 (January 1988 to November 1995) and GEOS-STRAT (December 1995 to December 1997). These meteorological fields are provided on a sigma coordinate system with 20 vertical levels for GEOS-1, 1000–10 hPa, and 46 levels for GEOS-STRAT, 1000–0.1 hPa. For computational expedience, we degrade the vertical resolution for GEOS-STRAT by merging the vertical levels above the lower stratosphere, retaining a total of 26 levels. The sigma levels of the model are given by *Bey et al.* [2001a] and are similar for both GEOS versions in the troposphere. All meteorological data were regridded from 2° by 2.5° (latitude by longitude) to the horizontal resolution used here, 4° by 5°. We used version 5.02 of the GEOS-Chem model for transport (http://www-as.harvard.edu/chemistry/trop). This version of model transport conserves tracer mass, as described by *Wang et al.* [2004].

[16] The model uses the advection scheme of *Lin and Rood* [1996], and the moist convective mixing scheme of *Allen et al.* [1996b] applied to the GEOS convective updraft, entrainment, and detrainment mass fluxes from the relaxed Arakawa-Schubert algorithm [*Arakawa and Schubert*, 1974; *Moorthi and Suarez*, 1992]. These transport schemes were evaluated with a simulation of ^{222}Rn by *Allen et al.* [1996b] and of ^{210}Pb and ^{7}Be by *Liu et al.* [2001]. *Allen et al.* [1997] evaluated deep convective mixing in GEOS-1 and found that the locations of deep convection are reasonable, though their frequency is generally overestimated in the tropics. *Molod et al.* [1996] found that the seasonal shift in the Intertropical Convergence Zone (ITCZ) is well reproduced, but that the ITCZ is too broad. Interhemispheric mixing was examined with simulations of ^{85}Kr, and found to be satisfactory, with an exchange time of 1.0 a for GEOS-1 and 1.1 a for GEOS-STRAT [*Wang et al.*, 2004].

[17] The global average cloud optical depths (COD) in the GEOS-1 and GEOS-STRAT fields are too low by a factor of 4–5 as compared to satellite retrieval products for column COD from MODIS and ISCCP (H. Liu et al., Sensitivity of photolysis rates and key oxidants in the troposphere to cloud vertical distributions and optical properties in a global three-dimensional chemical transport model, manuscript in preparation, 2007). The tropical CODs are about a factor of two too low. By comparing simulations with clear sky and with clouds, Liu et al. found that the radiative effect of clouds on global mean OH is not very sensitive to the column COD, but that it is sensitive to the cloud vertical distribution. GEOS-1 and GEOS-STRAT fields have similar vertical distributions of clouds. Thus, although the CODs are significantly too low in GEOS-1 and GEOS-STRAT, this likely has little effect on global mean OH. We discuss the credibility of our model OH further below.

[18] The only sink for CO that we consider is reaction with OH. We do not simulate the uptake of CO by microorganisms since this pathway is uncertain and likely counterbalanced to some degree by the degradation of plant matter, as discussed in section 3.4. Tropospheric OH is calculated interactively in the model at every time step using a chemical parameterization scheme [*Duncan et al.*, 2000]. The parameterization is derived from the chemical mechanism described by *Bey et al.* [2001a], and the rate constant for reaction of CO with OH is taken from *Sander et al.* [2003]. The parameterized chemistry decreases the model run time as compared to the kinetic solver used by *Bey et al.* [2001a] by over a factor of 10, allowing us to perform sensitivity studies with decade-long simulations. Removal of CO by OH in the stratosphere is calculated using loss frequencies from a 2-d stratospheric model [*Schneider et al.*, 2000; D. Jones, personal communication, 2000]; the production rate of CO from CH_4 oxidation in the stratosphere is taken from the same model. About 3% of CO loss occurs in the stratosphere. The atmospheric loss of model CO varies from 2231 to 2366 Tg CO/a.

[19] The parameterization accurately represents OH predicted by a full chemical mechanism as a set of high-order polynomials in variables such as ozone, CO, NO_x, CH_4, NMHC, H_2O, temperature, ozone column, and latitude

[*Duncan et al.*, 2000]. The model's zonal mean OH for January and July 1994 is shown in Figure 1. Meteorological and physical variables needed by the parameterization (e.g., temperature, pressure, H_2O) are taken from the assimilated meteorology. Chemical variables (e.g., ozone, NO_x, isoprene) are monthly averages from a simulation of GEOS-Chem with the kinetic solver for 1988 to 1997 [*Duncan and Bey*, 2004]. The monthly mean surface albedo in the ultraviolet is taken from *Herman et al.* [1999]. Methane mixing ratios are specified as annual mean values for 1988–1997 using NOAA/GMD measurements from remote sites [*Dlugokencky et al.*, 1998], and assumed to be uniform vertically and longitudinally in four semihemispheres. We allow for seasonal and interannual variability in the ozone column, using monthly mean vertical ozone profiles from *Logan* [1999a, 1999b] that are scaled to gridded monthly data for the total column (http://code916.gsfc.nasa.gov/Data_services/merged/data/toms_sbuv.v3.78-02.5x10.v7.txt) [*Fioletov et al.*, 2002].

[20] The radiative and heterogeneous chemical effects of aerosols were accounted for using the results of *Martin et al.* [2003] and a 3-D global distribution of aerosols from *Chin et al.* [2002] for September 1996 to August 1997. By relating the distributions of OH of Martin et al. with and without aerosols we obtained a set of correction factors for the parameterization. Typical correction factors at the surface of the Sahara Desert reduce OH by 55–90% in July and up to 80% over parts of India; reductions are 13% and 4% on average in the Northern and Southern Hemisphere (SH), respectively [*Martin et al.*, 2003].

[21] Our global mean tropospheric OH for 1988 to 1997 is $0.87–0.93 \times 10^6$ molecules/cm^3. The atmospheric lifetime for CH_3CCl_3 is 4.7–5.0 a, calculated using a lifetime of 34 a with respect to loss in the stratosphere [e.g., *Volk et al.*, 1997] and 80 a for uptake by the oceans [*Butler et al.*, 1991]. *Prinn et al.* [2005] reported an atmospheric lifetime of 4.9 (±0.3) a and *Spivakovsky et al.* [2000] reported 4.6 a. The lifetimes with respect to tropospheric OH in the present study are 5.8–6.3 a, 5.8–6.3 a in the SH and 5.7–6.3 a in the NH; these values are for the entire atmospheric burden of CH_3CCl_3, assuming a uniform mixing ratio. Our lifetimes are similar to that given for tropospheric loss by Prinn et al., 6.0 (+0. 5, −0.4) a, and Spivakovsky et al., 5.7 a.

3. Sources of CO

[22] The overall budget for model CO from 1988 to 1997 in the present version of GEOS-Chem is given in Table 1. The typical tropospheric burden is ~350 Tg in January and ~305 Tg in July. Here we discuss the magnitudes, spatial distributions, and the seasonal and interannual variations of the sources, and we highlight some of the reasons for differences between our emission inventories and those used in other studies. We discuss the IAV of the CO sink and its causes in Duncan and Logan (manuscript in preparation, 2007).

3.1. Emissions of CO From Fossil Fuel Combustion and Industry

[23] We used the same emissions from fossil fuel and industry as *Wang et al.* [1998] and *Bey et al* [2001a]. This inventory was developed in the early 1990s for the base year of 1985. Emissions for later years were scaled to emissions in 1985 as described below. Since the development of the inventory was described only briefly by *Wang et al.* [1998], we give more details here. We also provide comparison to the EDGAR2 inventory for CO for 1990 [*Olivier et al.*, 1996, 1999] and to the EDGAR3 inventories for 1990 and 1995 [*Olivier et al.*, 2001], which have been used in several studies of CO, and to the inventories of *Streets et al.* [2003, 2006] for Asia in 2000. We highlight the important sources of uncertainty in this large CO source. The inventory may be obtained by contacting J. A. Logan.

3.1.1. Emissions of CO in 1985

[24] The standard method for estimating emissions from fossil fuel and industrial activity is to multiply the combustion rate, or activity level, by an emission factor (EF) for the particular use. Emission factors for CO depend on the efficiency of combustion, and values vary by a factor of at least 300. For example, very little CO is produced by electricity generating plants that are designed to be efficient combustors, while large quantities are produced by unregulated internal combustion engines. Clearly, detailed information is required on how fuels are used. The principal global sources from fossil fuel combustion are gasoline vehicles and residential use of coal [*Logan et al.*, 1981; *Veldt*, 1991].

[25] Emissions were developed on a national basis. They were spatially disaggregated using a population map with resolution of 1° latitude × 1° longitude that we developed, as described by *Benkovitz et al.* [1996]. Emissions from fossil fuel and industry for the United States (U.S.) and Canada in 1985 were taken from the Environmental Protection Agency (EPA) Trends Report [*U.S. EPA*, 1994], and were spatially disaggregated with the same pattern as the NAPAP (National Acid Precipitation Assessment Program) inventory for 1985 [*U.S. EPA*, 1989]. The U.S. source from fossil fuel/industry given by *U.S. EPA* [1994] for 1985, 95 Tg CO/a, is significantly higher than that given by *U.S. EPA* [1989], 55 Tg/a, because of changes in estimates of past emissions from transportation made by EPA in the early 1990s.

[26] For the global inventory, fossil fuel statistics were taken from an electronic database compiled by the United Nations (UN) Office of Energy Statistics which gives consumption data by country for each fuel (e.g., coal, lignite, gasoline, diesel) in 32 categories (e.g., power plants, road transport, household). The breakdown of fuel use by categories is missing for some countries, including China, and for these cases we supplemented the UN data with fuel statistics provided the International Energy Agency (IEA) of the *Organization for Economic Development and Cooperation* (*OECD*) [1990, 1991a]. The statistics given by the IEA for China appear to be taken directly from the Chinese national statistics. *Bashmakov* [1992] was used for the breakdown of fuel use in the former Soviet Union (FSU), as this information was not provided by the UN energy statistics. If no specific information could be found for the consumption pattern for individual fuels in a given country, we used regional averages.

[27] We considered four categories of coal and lignite use: residential combustion, electricity and heat generation, conversion to coke, and all other uses (total consumption minus the first three). In 1985, on a global basis, 11% of

Table 3. Emission Factors for Solid Fuel[a]

	This Study	EDGAR2	*Streets et al.* [2003], China
Residential	5000	3800–6000	3400
Power plants	15	15–20	–
Coke	25		–
Other/industrial	100	20–150	–
Other/industrial in China	2500	150	1700

[a]Unit is g CO/GJ.

solid fuel was used in residences, 15% was converted to coke, 52% was used to generate power, and 22% was used in other ways. In North America and Europe coal is used primarily to generate electricity, and very little is used in residences. In China 25% of coal was consumed in residences and 45% by industry, primarily by small users, in 1985. Emission factors adopted for coal are given in Table 3; they are similar to values used in the EDGAR2 inventory. The value for residential use was taken from *Veldt* [1991]; 5000 g/GJ corresponds to about 9% of the carbon being emitted as CO. Emission factors for the other categories were taken from the EPA's compendium, AP-42 [*U.S. EPA*, 1985, 1993], and from values recommended for the European CORINAIR inventory [*Bouscaren*, 1991]. It seemed inappropriate to use EFs measured in developed countries (see Table 3) for industrial combustion in China in 1985, since at that time thermal efficiencies were low, units were small, and technology often dated back to the 1930s and 1940s [*World Bank*, 1985]. We arbitrarily selected an EF of 2500 g/GJ, half that for residential use, for China alone. *Streets et al.* [2003] adopted an EF of 3400 g/GJ for residential use of coal in China, based on the more recent measurements by *Zhang et al.* [1999, 2000], and they used half this value for industrial use of coal in China.

[28] Residential use of coal provides the largest source of CO from solid fuel. In 1985, 68% of the residential combustion of coal occurred in China (42%) and the FSU (26%), while 20% occurred in Poland, North and South Korea, and East Germany. The other large source from coal is from industry in China, but this is based on a rough estimate for the EF.

[29] Emissions from motor vehicles are typically calculated by models such as MOBILE in the U.S. [*U.S. EPA*, 1985] and COPERT in Europe [*Samaras and Zierock*, 1989]. These models use as input EFs given in g/km for different vehicle types (passenger cars, light and heavy trucks, etc). Since EFs depend on driving patterns, speed, temperature, age of vehicle, control technology, and quality of maintenance, these models require detailed input for these variables, as well as vehicle statistics and distance driven [e.g., *Sawyer et al.*, 2000]. We chose instead to use EFs given in terms of fuel consumption, i.e., gm CO/kg fuel. There are two advantages to this approach: gasoline statistics are more readily available on a global basis than information on distance driven, and emission rates are more constant on a fuel basis than on a distance basis [*Sawyer et al.*, 2000].

[30] We used EFs from the COPERT model given by *Samaras and Zierock* [1989] for both gasoline and diesel vehicles for 12 Western European countries. They give national EFs in terms of g CO/kg, as well as g/km. For most other parts of the world, we relied on EFs for unregulated vehicles [*U.S. EPA*, 1985; *Samaras and Zierock*, 1989], and knowledge of the predominant type of vehicle in various countries (e.g., light trucks in China [*World Bank*, 1985]). Emission factors adopted for gasoline in our inventory are given in Table 4, and are compared to those used in the EDGAR2 inventory by *Olivier et al.* [1996, 1999]. The EDGAR2 inventory used EFs for gasoline provided by Samaras for 1990, and they are rather similar to those used here. Values given by *Samaras and Zierock* [1989] for diesel vehicles in 1985 are about a factor of two smaller than those recommended for 1990 (Table 4). However, diesel fuel is a relatively small source of CO compared to gasoline.

[31] Our inventory did not include a source of CO from kerosene and diesel use (mixed with gasoline) in two-stroke engines in India, as proposed by *Dickerson et al.* [2002]; they estimate that the appropriate EF for vehicles in India is 800 g CO/kg. *Streets et al.* [2003] used a version of the MOBILE model to estimate emissions from motor vehicles in Asia. Their estimate of emissions from gasoline vehicles in China, combined with national gasoline use from the *National Bureau of Statistics of China* [1998], implies an average EF of about 1000 g CO/kg. We derive the same average value from estimates of vehicular emissions for Chinese cities given in *Fu et al.* [2001], whose work is the basis of the estimates by *Streets et al.* [2003]. These values are much higher than those we adopted for developing countries, 450–520 g CO/kg (Table 4).

[32] The national average EF given in Table 4 for gasoline vehicles in the U.S. was calculated from CO emissions given by *U.S. EPA* [1994] and total gasoline use in the U.S. given by the *Department of Transportation* (*DOT*) [1986]. It is about 30% smaller than values in Western Europe because vehicle emissions were regulated starting in the 1970s in the U.S., but not until the 1980s in Europe. We include the U.S. value for comparison purposes; it was not used in the inventory. Gasoline use in the U.S. and Western Europe accounted for 64% of global use in 1985.

[33] Industrial processes provided 9% of the total source of CO in the U.S. prior to regulation (pre-1970) [*U.S. EPA*, 1992], and 19% of the source in West Germany [*Welzel and Davids*, 1978]. The largest contributor in both countries was the iron and steel industry, with carbon black production

Table 4. Emissions Factors for Gasoline[a]

	This Study 1985	EDGAR2 1990[b]
United States	265[c]	258
W. Europe (country specific)	376.5[d] (300–470)	346
USSR/CIS	518	538
Other E. Europe	480	588
China	520	467
Japan	154	160
Australia, New Zealand	376.5	291
Other	450	450–610

[a]Unit is g/kg.
[b]Average values for region. Country specific values were used.
[c]National average calculated from on- and off-road emissions from gasoline for the U.S. for 1985 [*U.S. EPA*, 1994] and total gasoline use in the U.S. [*DOT*, 1986].
[d]Average values for region. Country specific values were used for 12 countries.

Table 5. Emission Factors for Industrial Processes

	This Study, g CO/kg	EDGAR2, 1990, g CO/kg
Iron and steel		
Basic oxygen[a]	16 (69)	15
Electric arc[a]	9(30)	10
Open hearth	70	50
Sinter	30	25
Blast furnaces	2	10
Iron foundries[a]	72.5 (450)	
Catalytic cracking of petroleum[b]	1.56–9 (39.2) kg/10^3 l	
Carbon black[c]	1525	
Primary aluminum smelting	164	4
Kraft pulp and paper	20.5	

[a]Values in parentheses were used in the USSR, Eastern Europe and China.

[b]1.56 kg/10^3 l was used for the U.S. and Japan, 39.2 kg/10^3 l was used for the FSU and China and values of 6–9 kg/10^3 l elsewhere, based on data from *U.S. EPA* [1985, 1989], and D. Mobley (personal communication, 1992). Values given are for fluidized bed catalytic cracking.

[c]Assumes 90% produced by the oil furnace process (EF = 1400 g/kg) and 10% by the gas process (EF + 2650 g/kg) as in the U.S. in 1985.

and catalytic cracking of petroleum providing important sources in the U.S. Emissions of CO from these processes are controlled in the U.S., to conserve energy and reduce air pollution. The degree of control was unknown for most countries, so educated guesses were made. Emissions from other minor industrial processes were made using EFs for the U.S. [*U.S. EPA*, 1985, 1991].

[34] Emission factors adopted here are given in Table 5. Values for the iron and steel industry are based on those used in the national inventories for the U.S. [*U.S. EPA*, 1985, 1991], West Germany [*Welzel and Davids*, 1978; C. Veldt, personal communication, 1992], and East Germany [*Bethkenhagen et al.*, 1988]. We selected the higher of the two EFs used in the U.S. and West Germany for most countries. Uncontrolled EFs from *U.S. EPA* [1985], or the values recommended for East Germany, were adopted for the FSU, Eastern Europe, and China. Emissions were estimated using national statistics for sinter production, pig iron, scrap iron and steel, and for crude steel production by furnace type [*International Iron and Steel Institute*, 1987; *World Bank*, 1985; *U.S. Bureau of Mines*, 1987; *United Nations*, 1991]. Emissions from other industries were calculated with production data from the Industrial Statistics Yearbook [*United Nations*, 1991]. Our emission estimates for CO from industrial processes are summarized in Table 6. The iron and steel industry emits 50 Tg CO, while other industries emit 16 Tg CO.

Table 6. Emissions CO From Industrial Processes in 1985

	Production, Tg	Emissions of CO, Tg CO
Iron and steel industry		
Sinter	560	16.7
Basic oxygen	400	9.5
Electric arc	179	2.2
Open hearth	140	9.8
Pig iron in blast furnaces	500	1.0
Foundries: pig iron/scrap	52	11.2
Subtotal		50.4
Catalytic cracking of petroleum	502	3.3
Carbon black	1	6.8
Primary aluminum	15	2.5
Kraft pulp and paper	76	1.5
Organic chemicals		
Ammonia	86	8
Total		66.5

Table 7. Global Emissions of CO From Fossil Fuel and Industry

Sector	CO, Tg/a
Gasoline vehicles	232
Solid fuel: residential	53
Solid fuel: all other uses	22
Iron and steel industry	50
Other industry	16
Diesel vehicles	6
Diesel: other uses	4
Total[a]	390

[a]The total includes other sectors from the U.S. and Canadian inventories, including wood fuel (~6 Tg) and waste disposal (~2 Tg).

[35] Our estimate of CO emissions from fossil fuel and industry for 1985 is 390 Tg, with a breakdown by sector given in Table 7 and a regional breakdown in Table 8. This estimate uses national emission estimates for the U.S. and Canada [*U.S. EPA*, 1994], rather than the EFs given in Tables 2–4; because of this, our total of 390 Tg includes 7 Tg CO from use of wood fuel in the U.S. and Canada. Gasoline use provided the largest source, 232 Tg CO, followed by residential use of coal, 53 Tg, and the iron and steel industry, 50 Tg. North America provides the largest regional source, 28%, followed by the FSU and Eastern Europe, 25%, and Western Europe and Japan, 18%. Only 5% of emissions are in the SH.

[36] Our estimate of CO emissions from fossil fuel in 1985, 317 Tg, is larger than that in the EDGAR2 inventory for 1990, 263 Tg, as is our estimate for emissions from industry, 66 Tg verses 35 Tg. We compare our estimates with those of the EDGAR2 inventory in Table 9, using their sectors [*Olivier et al.*, 1999]. Our estimates are larger for all sectors, with differences of less than 15% for transportation and residential use of fuel. Our estimate is significantly larger for other uses of solid fuel, because of the high EF we adopted for industrial use on China. It is 30% larger for the iron and steel industry. The EDGAR2 inventory omitted other industrial processes that generate CO, except for aluminum production, a minor source. The source of CO from fossil fuel and industry in the more recent EDGAR3.2 inventory is 319 Tg for 1990, 20 Tg larger than their earlier estimate; the EDGAR3.2 estimate for 1995 is 310 Tg for 1995 [*Olivier et al.*, 2001]. The EDGAR inventories rely on energy statistics from the IEA/OECD. These inventories, and that of *Streets et al.* [2003], are developed in more detail for some CO sources, such as transportation, but the same fundamental uncertainties remain in EFs.

[37] *Holloway et al.* [2000] developed an inventory for CO by scaling the NO_x inventory for 1985 of *Benkovitz et al.*

Table 8. CO Emissions by Region

	CO, Tg
U.S. and Canada	110
FSU and E. Europe	97
W. Europe and Japan	71
China	55
Other N. Hemisphere	37
Other S. Hemisphere	20
Total	390

[1996]. They first extrapolated the NO_x inventory from 1985 to 1990 using energy statistics, and substituted the Asian NO_x emissions of *van Aardenne et al.* [1999]. They used a molar CO:NO_x ratio of 6.7, derived from the EPA inventory for the U.S. in 1990, to convert NO_x to CO. This procedure gives an estimate of 300 Tg CO, similar to the EDGAR inventory, but must give a different spatial distribution.

[38] We compared our results to those of regional inventories for fossil fuel and industrial sources of CO. Our estimate for European countries is 8% larger than values given for 1985 in the EMEP database [*Vestreng and Storen*, 2000], and 10% larger than the CORINAIR European inventory for 1990 [*U.S. EPA*, 1994]. Our estimate for China, 56 Tg, is much larger than that given by *Streets and Waldhoff* [2000] for 1990, 32 Tg. *Streets et al.* [2003] provide an estimate for Chinese emissions of 64 Tg for 2000, and comment that emissions have likely been stable in recent years. In a new study, which focuses on improving estimates particularly for the industrial sector, *Streets et al.* [2006] give an estimate of 101 Tg for China in 2001. The estimate for China (and a few Asian countries with small emissions) in EDGAR2 is 35 Tg. Our estimate for the FSU is 74 Tg, EDGAR2 gives 46 Tg, EMEP gives 29 Tg, and *Bashmakov* [1992] gives 44 Tg for 1988. In this case, our estimate is larger than that of EDGAR2 mainly because of differences for transportation (14 Tg) and the iron and steel industry (12 Tg). On a global basis, 60% of the difference in our estimate and that of EDGAR2 arises from values for China and the FSU.

[39] There have been very few estimates of global CO emissions from fossil fuel and industry, although many secondary sources have been cited in the literature and in Intergovernmental Panel on Climate Change (IPCC) and World Meteorological Organization (WMO) assessments, with a range of 300–550 Tg appearing in recent reports [*Intergovernmental Panel on Climate Change*, 1996; *WMO*, 1999]. The estimates from earlier inventories are as follows: 360 Tg for 1970 [*Jaffe*, 1973]; 640 Tg for 1971, based on adding a rough estimate of other sources to the work of Jaffe [*Seiler*, 1974]; 440 Tg for 1976 [*Logan et al.*, 1981]; and 784 Tg for 1979 [*Cullis and Hirschler*, 1989]. Cullis and Hirschler's total is so high in part because they estimate that the petroleum refineries produce 256 Tg CO, a factor of 80 larger than our estimate for this industry. Omitting this source from Cullis and Hirschler, the primary estimates are in the range 360 to 530 Tg for 1970 to 1979.

[40] How reliable are estimates of global CO emissions from fossil fuel and industry? The greatest source of uncertainty lies in the EFs, most of which were measured or estimated for conditions in the U.S. and Europe. If the estimates for CO from transportation in the U.S. and Western Europe are reliable for 1985, this implies that we could be confident about emissions from 65% of the world's gasoline use. In a recent review of the U.S. situation, *Sawyer et al.* [2000] conclude that large and significant uncertainties exist in current mobile source emissions inventories, and that they exist for all vehicle types. Their review of tunnel studies shows a range of a factor of two in CO EFs for 1992–1995, 53–123 g CO/kg for light duty vehicles. Another difficulty in making reliable estimates is that the distribution of emissions is highly skewed, with 10% of the vehicles (usually those about 10 a old) providing 50% of CO emissions. Other sources of error are that the EFs in g/km are derived from laboratory measurements of a specific driving cycle that do not adequately characterize real world conditions, and that information on vehicle activity is not necessarily accurate [*Sawyer et al.*, 2000]. The same difficulties are only magnified when making estimates for developing countries, when issues such as poorly maintained vehicles and adulteration of fuel must be considered [*Dickerson et al.*, 2002], as well as slow speeds caused by congestion in megacities. *Beaton et al.* [1992] found that average emissions of vehicles in Mexico City were 475 g CO/kg, larger than unregulated vehicles in the U.S., and that in Mexico 25% of the vehicles provided 50% of the emissions. In a similar study, *Bradley et al.* [1999] reported even higher values for Nepal and Thailand.

[41] Recent measurements of CO emissions from coal-burning household stoves in China give a mean EF of 3400 g/TJ with a range of 1150–7500 g/TJ [*Zhang et al.*, 2000], suggesting our mean value for residential combustion of 5000 g/TJ may be high, but also indicating large uncertainty. It is also likely that emission factors in China may be different from those for residential combustion of coal in Russia and Eastern Europe. Another potential source of error lies in assuming that industrial combustion is highly efficient globally, emitting very little CO as in the U.S. and Western Europe. We showed above that this could be an important source in China, but data are lacking for small-scale industrial combustion in the developing world. Similarly, the emissions from the iron and steel industry could be significantly in error. Coke oven batteries and blast furnaces generate large amounts of CO, which is used as a fuel, and the EFs for the U.S. and Western Europe assume that little of this escapes to the atmosphere. This may not be the case for older technology used in Eastern Europe and China. Indeed, the latest analysis by *Streets et al.* [2006] focuses on estimating emissions from small-scale industry in China, including inefficient combustion of coal in small devices such as kilns, and production of coke, iron, and steel, and it is these sectors that are responsible for most of the increase in emissions compared to their previous work [*Streets et al.*, 2003].

[42] Another potential source of error in estimating emissions from China is the underlying energy statistics, which show a decline in coal use starting in 1996. *Sinton* [2001] argues that the statistics are relatively good for the early 1990s, but that their quality has declined since the mid 1990s.

3.1.2. Emissions of CO From Fossil Fuel and Industry in 1988 to 1997

[43] Emissions for individual countries were scaled from the 1985 values in the base inventory as described by *Bey et al.* [2001a]. We used annual emissions estimates provided by *U.S. EPA* [1997] for the U.S. and by *EMEP* [1997] for European countries for the scaling factors. For countries without emission regulations, we scaled CO emissions for a particular year to carbon dioxide (CO_2) emissions from liquid fuels [*United Nations*, 1998; *Marland et al.*, 1999]. This approach is reasonable for most countries where transportation provides the largest source of CO. For China, where most CO emissions in 1985 were from coal combustion, this approach increased the source from 55.5 Tg in

Table 9. Comparison of Estimates for CO Emissions From Fossil Fuel and Industry

	CO, Tg, 1985, This Work	CO, Tg, 1990, EDGAR2
Road transport	238	208
Residential fuel	53	49
Other fossil fuel combustion	26	6
Iron and steel industry	50	35
Other industry	16	0

1985 to 68 Tg in 1988, and to 103 Tg in 1997, an increase by a factor of 1.88 in 13 a. We were concerned that this might be an overestimate. Although transportation was not a major source in China in 1985, gasoline use increased by a factor of 2.4 between 1985 and 1997 [*China Statistical Information and Consultancy Service Centre*, 1988; *National Bureau of Statistics of China*, 1998]. If we had adopted the mean EFs for coal combustion and gasoline use in China used by *Streets et al.* [2003], our estimate for 1985 would be 50 Tg CO; employing the trends in coal use by sector in China shown by *Sinton and Fridley* [2000] and in gasoline use given above would lead to an increase by a factor of 1.66 in 1997, to 82 Tg CO. This is smaller than the increase used here by only 16 Tg.

[44] The total direct annual emissions of CO from fossil fuels and industry decreased from 411 Tg in 1988 to 391 Tg in 1995, and increased slightly to 404 Tg in 1997 (Figure 2). Emissions decreased by only 2–3% globally over the decade, as increases in eastern Asia of 51% caused by rapid economic development were offset by declines in Europe and North America. The largest decline was in Eastern Europe (45%) caused largely by economic contraction of the FSU. There were smaller declines in Western Europe (32%) and North America (17%) caused primarily by increasing levels of emissions control on vehicles. The implications of these regional changes in emissions on CO are discussed by Duncan and Logan (manuscript in preparation, 2007).

[45] Production of CO from the oxidation of anthropogenic NMHC provides an extra 72–76 Tg CO/a, bringing the total source from fossil fuels/industry to 464–487 Tg/a. The method used to estimate CO from anthropogenic NMHC is described in section 3.6.

[46] The seasonal variation of fossil fuel emissions of CO and NMHC is caused in part by emissions from transportation. We estimate that the emissions from cars in winter are about 14% higher than the annual mean and about 14% lower in summer. Our estimate accounts for the enhanced vehicle emissions of CO and NMHC in winter because the efficiency of emission control devices are temperature-dependent [*Stump et al.*, 1989] and the higher number of total vehicle miles traveled during the summer months [*Federal Highway Administration*, 2001]. Since mobile sources contribute 57% of the total emissions from the U.S. [*U.S. EPA*, 2000], our estimate of the seasonal variation in fossil fuel emissions is ±8% about the annual mean. We vary the fossil fuel emissions north of 30°N latitude in the model accordingly. This estimate of the seasonal variation in fossil fuel emissions is likely to represent the variation in emissions for Europe, but may be an underestimate in China where coal is used for heating in winter. *Streets et al.* [2003] estimate that emissions from China are much higher in November to February than in the rest of the year, because of residential use of coal and biofuel for heating. Their work suggests that we may be underestimating the seasonality of emissions north of 30°N by at least a factor of two. We chose not to impose seasonality for the residential sector as our estimate is rather uncertain because of the paucity of data for emission factors.

3.2. Biofuels

[47] Emissions of CO from biofuels were estimated from the inventory and EFs of *Yevich and Logan* [2003]. Biofuels included in the inventory are fuel wood, charcoal, agricultural residues and dung. The annual emission rate in the developing world is 159 Tg/a, to which we add 30 Tg/a from photochemical oxidation of NMHC produced by biofuel combustion (Table 1). We assume no seasonal variation in biofuel use, as these fuels are used largely in the tropics for cooking. There is likely some seasonal variation in use for heating at high altitudes in the tropics, and in northern China. The EDGAR2 inventory gives a global source of 181 Tg in 1990, while EDGAR3.2 gives 216 Tg for 1990 and 232 Tg in 1995, with only 15 Tg of this in the developed world [*Olivier et al.*, 1996, 1999]. We do not allow for IAV in biofuel combustion. Emissions may have increased by as much as 20% in the tropics from 1985 to 1995 [*Yevich and Logan*, 2003], but Chinese statistics suggest a decrease since 1990 [*Streets et al.*, 2001].

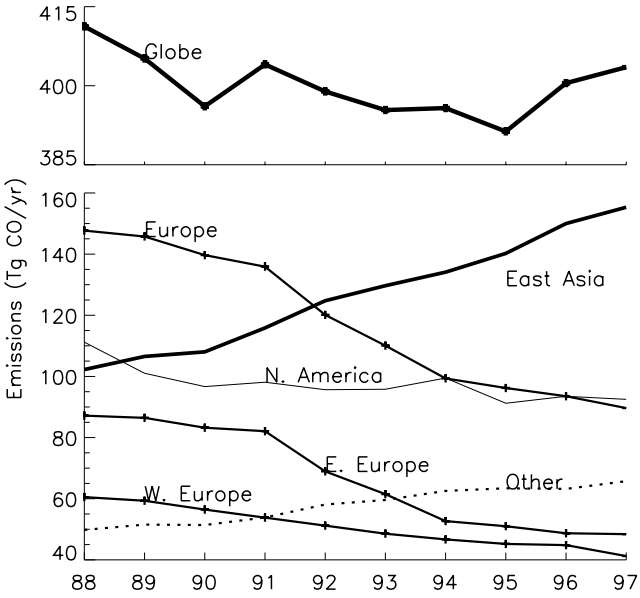

Figure 2. Total direct emissions (Tg CO/a) from fossil fuel use and industry from Europe (solid line with plus symbols; 38–70°N; 15°W–75°E and 52–70°N; 75°E–180°), North America (fine solid line; 28–70°N; 170–50°W), east Asia (heavy solid line; 8–44°N; 75–150°E), and the rest of the world (dashed line). The global total is shown as a heavy solid line with plus symbols. The emissions from Eastern Europe (>22°E) and Western Europe (<22°E) are also shown (solid lines with plus symbols).

3.3. Biomass Burning

[48] One of the largest uncertainties in the budget of CO is the magnitude of emissions from biomass burning, as well as its IAV. Estimates ranged from 450 to 920 Tg CO/a in the model intercomparison of *Kanakidou et al.* [1999]. *Galanter et al.* [2000] showed that six estimates used in CTMs vary from 3260 to 10,450 Tg DM (dry matter) burned annually.

[49] The emissions inventory used in this study is summarized by *Lobert et al.* [1999] and *Duncan et al.* [2003a], with a detailed assessment of agricultural waste burning given by *Yevich and Logan* [2003]. Categories in the inventory are deforestation, shifting cultivation, agricultural residues burned in the field, savanna burning, and forest fires. A total of 5525 Tg DM is consumed annually, representing a mean for 1980 to 1990. This is larger than the estimate of *Hao and Liu* [1994] for tropical burning, 4610 Tg DM/a, which was used in the EDGAR2 inventory. Emissions were determined by applying EFs for each of the above categories to give a mean emission rate of 437 Tg CO/a [*Duncan et al.*, 2003a].

[50] We constrained the timing of emissions as described by *Duncan et al.* [2003a]. Specifically, we used the Total Ozone Mapping Spectrometer (TOMS) Aerosol Index data (AI) product [e.g., *Herman et al.*, 1997; *Torres et al.*, 1998] and fire counts from the Along Track Scanning Radiometer (ATSR) World Fire Atlas [*Arino and Rosaz*, 1999] as surrogates for the timing of biomass burning. For Africa only, the timing of burning was based on a climatology due to limitations of the method of *Duncan et al.* [2003a]. The spatial pattern of burning within each region was the same for 1988 through mid-1996, but it varied from mid-1996 through 1997 on the basis of the locations of fire counts, except in Africa, as discussed by *Duncan et al.* [2003a]. In contrast to *Yung et al.* [1999], we found no large-scale, long-term trends in biomass burning during our simulation period, but that there is significant IAV. Our source varies from 406 to 516 Tg CO/a from 1988 to 1997, with highest emissions in 1991, 1994, and 1997. Adding 45–57 Tg/a from the oxidation of NMHC associated with biomass burning brings the totals to 451–573 Tg/a (Table 1; see section 3.6).

3.4. Direct Emissions That Were Not Included

[51] We do not simulate the direct emission of CO from plants, degrading plant matter, or the ocean since these pathways are uncertain and the magnitudes of these sources are relatively small. Recent estimates of the emissions from plants and degrading organic matter range from 75 to 380 Tg/a [*Kanakidou et al.*, 1999, and references therein]. We expect these emissions are roughly balanced with the amount consumed by soils, 115–240 Tg/a [*Sanhueza et al.*, 1998], and that they exert no significant net influence on CO. Measurements of CO in the surface ocean typically indicate supersaturation with respect to equilibrium, indicating an oceanic source, with estimates as high as 120 (±80) Tg/a in the literature [e.g., *Linnenbom et al.*, 1973; *Seiler*, 1974; *Seiler and Schmidt*, 1974; *Conrad et al.*, 1982]. *Bates et al.* [1995] reported an ocean source at the low end of previous estimates, 6–30 Tg/a, based on analysis of data from six trans-Pacific cruises. We believe these estimates to be reliable.

3.5. Methane Oxidation

[52] The source of CO from CH_4 oxidation is calculated using measurements of specified mixing ratios of CH_4 (section 2.1), OH calculated by the parameterization scheme, and the rate constant for CH_4 + OH given by *Sander et al.* [2003]. Production rates in the stratosphere were calculated off-line with a 2-D model [*Schneider et al.*, 2000; D. B. Jones, personal communication, 2000]. We assume that the yield of CO per molecule of CH_4 oxidized, α_{CH4}, is 1.0. We find that production ranges from 778 to 861 Tg CO/a from 1988 to 1997, about one third of the total source (Table 1). Only 2% of this source lies in the stratosphere.

[53] Values reported for α_{CH4} are significantly lower than unity. *Logan et al.* [1981] gave a value of 0.78, assuming that intermediate products are removed efficiently by wet deposition. Solubility data for methylhydroperoxide, CH_3OOH, and formaldehyde, CH_2O, were lacking until the mid-1980s [*Lind and Kok*, 1986; *Bretterton and Hoffmann*, 1988]. *Tie et al.* [1992] reported an α_{CH4} of 0.82 on the basis of the assumptions of *Logan et al.* [1981]. *Manning et al.* [1997] deduced a value of 0.7 from measurements of CO isotopes in the SH, while *Bergamaschi et al.* [2000b] estimated an a posteriori average α_{CH4} of 0.86 in an inversion study of CO isotopes. *Novelli et al.* [1999] examined the yields of H_2 and CO from CH_4 oxidation and proposed a mean $\alpha_{CH4} = 0.95$, with 5% of CH_2O lost to dry deposition.

[54] We assume α_{CH4} to be 1.0 for both high- and low-NO_x chemical environments [*Kleinman*, 1994], on the basis of the following considerations. In a high-NO_x environment, oxidation of CH_4 leads rapidly to production of CH_2O without involving relatively long lived intermediates. Formaldehyde has a Henry's law constant that puts it on the threshold of efficient scavenging in deep convective clouds [*Mari et al.*, 2000], but there are no observations that provide evidence of significant scavenging in clouds or fogs [*Jacob*, 2000]. Its photochemical lifetime is hours, shorter than the typical frequency of deep convective events. The lifetime with respect to deposition is long (~months). Thus CH_2O is likely to photolyze or to react with OH, leading to a yield of 1 for CO. In a low-NO_x environment, oxidation leads to the production of CH_2O via CH_3OOH, a relatively long lived intermediate. Wet scavenging of CH_3OOH is likely small because it has low solubility [*Magi et al.*, 1997]; it will photolyze or react with OH, producing CH_2O, and a yield of 1 for CO. In a sensitivity study, we found that reducing α_{CH4} to 0.9 in our model results in a decrease in CO of <5 ppbv globally, and by <10% in the tropics and SH where CH_4 oxidation is a major contributor to total CO.

3.6. Secondary Production From NMHC

[55] The oxidation of NMHC provides an important source of CO [*Zimmerman et al.*, 1978; *Logan et al.*, 1981; *Kanakidou and Crutzen*, 1999; *Granier et al.*, 2000]. We account for NMHC emitted by fossil fuel use and industry, biofuels, biomass burning, and vegetation. Production is derived by multiplying the emission rate of each NMHC by a yield of CO per carbon oxidized (α_{NMHC}), with yields taken from *Altshuller* [1991] (Table 10); individual α_{NMHC} do not account for the loss

Table 10. NMHC Emissions Budget With Total Production of CO by Oxidation

Chemical Tracers	Biogenics,[a] Tg C/a	Biomass Burning,[b] Tg C/a	Biofuels,[b] Tg C/a	Fossil Fuels,[a] Tg C/a	Sum, Tg C/a	α_{NMHC}[c]	Total Production, Tg CO/a
Ethane	–	1.9	2.6	5.2	9.7	0.56	12.6
Propane	–	0.7	1.2	5.5	7.4	0.61	10.5
$\geq C_4$ alkanes	–	0.6	0.78	24	25.8	0.50–0.72	31.3
$\geq C_3$ alkenes	–	3.9	6.5	7.8	18.0	0.25–0.74	25.2
Formaldehyde	–	1.9	0.50	0.0	2.4	1.00	5.5
$\geq C_3$ aldehydes	–	2.6	0.67	0.0	3.3	0.49–0.56	3.9
Acetone	16	1.8	0.5	0.85	19.1	0.67	29.9
$\geq C_4$ ketones	–	3.6	1.4	0.81	5.8	0.54	7.3
Isoprene[d]	397	–	–	–	397	0.20[d]	180
Ethyne	–	1.6	1.3	–	2.8	0.60	3.9
Ethene	–	5.2	3.2	4.8	13.2	0.89	27.4
Alcohols	43[e]	3.6	1.6	–	48.7	0.68–1	109
Aromatics	–	3.2	5.7	10.9	19.8	0.09	4.2
Monoterpenes[f]	150	–	–	–	150	0.20	70
Total	606	30.5	25.9	60.0	723		521

[a]The fossil fuel and biogenic emissions are for 1994.
[b]The biofuel and biomass burning emissions are annual average emissions.
[c]Yield of CO per atom C of NMHC oxidized.
[d]Average yield is a function of the NO_x concentration; the range of yields is 0.16 to 0.42. The emission rate is dependent on solar radiation and temperature; based on the inventory of *Guenther et al.* [1995] with modifications described by *Wang et al.* [1998] and *Bey et al.* [2001a].
[e]Methanol only.
[f]The emission rate is dependent on temperature; based on the inventory of *Guenther et al.* [1995] with modifications described by *Wang et al.* [1998].

of intermediate trace gases by deposition, so we may overestimate some yields. The resulting CO is emitted directly, which may overpredict the contribution from longer-lived NMHC in source regions in winter. The assumption of immediate formation is more reasonable for the short-lived biogenic species, isoprene and monoterpenes. We find that anthropogenic NMHC contribute about 7% to the total source, while biogenic NMHC contribute about 15% (Table 1).

3.6.1. Anthropogenic NMHC

[56] Emissions were taken from the inventory of *Piccot et al.* [1992], which includes both fossil and wood fuels. For the latter they relied on vegetal fuel use statistics from the International Energy Agency [*OECD*, 1990, 1991b], which give significantly lower biofuel amounts than *Yevich and Logan* [2003]. We subtracted the biofuel emissions from the Piccot et al. inventory, so that we could use the biofuel inventory of Yevich and Logan. Biofuel emissions of 12 Tg C/a paraffins and 7 Tg C/a olefins were removed from the former inventory. We developed emissions estimates for biofuel and biomass burning by applying the EFs for individual NMHC compounds from *Andreae and Merlet* [2001] to the inventories described in sections 3.2 and 3.3. Applying the yields in Table 10, we find that oxidation of anthropogenic NMHC results in a source of CO that amounts to 19%, 19% and 11% of the direct emission of CO from fossil fuels/industry, biofuels and biomass burning, respectively. The direct emissions from these three source categories are increased by these amounts to account for the indirect source from oxidation of coemitted NMHC.

3.6.2. Biogenic NMHC

[57] Biogenic emissions of isoprene, monoterpenes, methanol, and acetone are included as sources of CO. These produce 354–379 Tg/a (Table 1). Their oxidation makes up 71% of the photochemical source from NMHC, with the remainder from fossil fuel (14%), biomass burning (9%), and biofuel sources (6%) (Table 10).

[58] Isoprene emissions are based on a modified version of the inventory of *Guenther et al.* [1995], and are dependent on solar radiation and temperature. The modifications are described by *Wang et al.* [1998] and *Bey et al.* [2001a]. The global isoprene emission rate of the modified inventory, 397 Tg C/a for 1994, is about 20% lower than the inventory of Guenther et al., 503 Tg C/a.

[59] The yield of CO from isoprene oxidation, α_{isop}, is dependent on local NO_x [*Miyoshi et al.*, 1994]. We estimated this yield using results from a CTM simulation with a carbon accounting scheme to track the carbon in isoprene oxidized to CO (A. C. Fusco, personal communication, 2000). We calculated $\alpha_{isoprene}$ according to the following equation: $\alpha_{isop} = 0.16 * [NO_x\ (ppbv)] + 0.12$, with a maximum α_{isop} of 0.42 and a minimum of 0.16. The global average value for α_{isop} is ~0.2 in our model, with values of 0.4 for polluted regions and generally <0.2 for clean tropical regions. The resulting production is ~170–184 Tg CO/a (Table 1), significantly lower than the estimates adopted by *Bergamaschi et al.* [2000a], 400 Tg/a, and *Holloway et al.* [2000], 648 Tg/a. They both used the unmodified inventory of *Guenther et al.* [1995], and they assume higher values for α_{isop}, 0.34 for the former and 0.55 for the latter (T. Holloway, personal communication, 2001).

[60] Monoterpene emissions are taken from *Guenther et al.* [1995] as modified by *Wang et al.* [1998]. The emission rate in the modified inventory, 150 Tg C/a, is about 18% higher than the original, 127 Tg C/a. The yield of CO from monoterpene oxidation, α_{mono}, is assumed to be 0.24 [*Hatakeyama et al.*, 1991; *Vinckier et al.*, 1998], giving emissions of 68–71 Tg CO/a for 1988–1997. The emissions given by *Bergamaschi et al.* [2000a] and *Holloway et al.* [2000] are taken from *Guenther et al.* [1995] (Tables 1 and 2). Holloway et al. assumed α_{mono} to be 0.08 and Bergamaschi et al., 0.33.

[61] *Singh et al.* [2000] estimated a methanol source of 28–79 Tg C/a of which about 19–47 Tg C/a is of biogenic origin with an additional 4–15 Tg C/a from decaying plant

Table 11. Statistical Comparison With Observations for the Base Simulation

Station ID	Station Location	Latitude, deg	Longitude, deg	Altitude, m	N[a]	Δ,[b] ppbv	Δ,[c] %	Standard Error,[d] ppbv	R[2e]	R_{ds}^{2f}	R_{dst}^{2g}	Trend Model,[h] %/a	Trend Data,[h] %/a
					High Northern Hemisphere								
ALT	Alert, Canada	82°N	62°W	210	67	4.8	4.2	1.5	0.88	0.29	0.12	−1.3 ± 0.5	−1.7 ± 0.6
MBC	Mould Bay, Canada	76°N	119°W	58	63	7.3	4.6	2.1	0.86	0.49	0.35	−1.4 ± 0.9	−1.2 ± 0.8
BRW	Barrow, Alaska	71°N	36°W	11	112	NS	NS	1.6	0.84	0.48	0.16	−1.8 ± 0.5	−1.9 ± 0.3
ICE	Heimaey, Iceland	63°N	20°W	100	59	6.2	5.3	1.9	0.75	NS[k]	NS	NS	NS
					Europe								
MHD	Mace Head, Ireland	53°N	9°W	25	79	9.9	8.2	2.6	0.66	0.45	0.45	NS	NS
HUN	Hegyhatsal, Hungary	46°N	16°E	248	57	NS	NS	6.1	0.62	NS	0.29	2.5 ± 1.0	−2.8 ± 2.0
					North America and North Atlantic								
CMO	Cape Meares, Oregon	45°N	123°W	30	62	7.7	7.5	2.6	0.62	0.16	0.12	−1.6 ± 1.1	NS
NWR	Niwot Ridge, Colorado	40°N	105°W	3475	107	NS	NS	1.4	0.51	0.10	0.10	−0.8 ± 0.3	NS
ITN	Grifton, North Carolina	35°N	77°W	505	66	−14	−6.0	4.1	0.29	0.07	NS	0.9 ± 0.7	NS
BMW	Southhampton, Bermuda	32°N	65°W	30	71	NS	NS	2.2	0.69	0.09	0.16	−0.7 ± 0.7	−1.9 ± 1.3
IZO	Tenerife, Canary Islands	28°N	16°W	2300	72	−7.6	−5.8	1.2	0.79	0.31	0.19	−1.0 ± 0.5	−3.1 ± 1.0
RPB	Ragged Pt., Barbados	13°N	59°W	3	69	NS	NS	1.1	0.66	0.22	0.22	−0.5 ± 0.5	−1.3 ± 0.9
					East Asia and North Pacific								
CBA	Cold_Bay, Alaska	55°N	162°W	25	69	−12	−9.0	1.4	0.85	0.12	NS	−0.9 ± 0.5	−0.8 ± 0.6
TAP	Tae-ahn, S. Korea	36°N	126°E	20	79	48	23	8.1	0.17	NS	NS	1.7 ± 1.2	NS
WLG	Mount Waliguan, PRC	36°N	100°E	3810	78	4.9	6.1	2.2	0.39	0.06	NS	NS	NS
MID	Sand Island, Midway	28N	177°W	4	72	−17	−13	1.3	0.90	0.17	0.20	−1.1 ± 0.9	NS
MLO	Mauna Loa, Hawaii	19°N	155°W	3397	102	−11	−11	1.1	0.72	0.09	0.05	−1.0 ± 0.5	−1.1 ± 0.8
GMI	Guam, Mariana Islands	13°N	144°E	2	99	−21	−19	1.6	0.55	0.21	0.16	−0.7 ± 0.6	−1.0 ± 1.0
GMI[i]					99	−14	−13	1.0	0.76	0.30	0.28	−0.7 ± 0.6	−1.1 ± 0.8
					Southern Hemisphere Tropics								
SEY	Mahe Island, Seychelles	4°S	55°E	3	80	−18	−19	1.5	0.73	0.40	0.37	NS	NS
ASC	Ascension Island	7°S	14°W	54	107	NS	NS	1.7	0.42	NS	NS	NS	−2.3 ± 0.8
ASC[i]					107	NS	NS	1.5	0.48	0.17	0.13	NS	−1.2 ± 0.7
SMO	American Samoa	14°S	170°W	42	112	−6.9	−10	0.68	0.27	0.29	0.31	NS	−1.0 ± 0.6
					Middle and High Southern Hemisphere								
CPT[j]	Cape Point, South Africa	34°S	18°E	210	120	−2.0	−2.9	0.43	0.71	0.14	0.18	0.34 ± 0.25	−0.37 ± 0.34
CGO	Cape Grim, Tasmania	40°S	144°E	94	78	1.8	4.9	0.70	0.54	NS	NS	NS	−0.8 ± 0.7
SYOv	Syowa, Antarctica	69°S	39°E	11	59	NS	NS	0.59	0.73	0.19	NS	1.4 ± 0.3	−2.0 ± 0.7

[a]N is the number of monthly mean observations coincident with model output.
[b]The bias is the mean of (model-observed)/observed for the entire time series.
[c]Mean bias (%) relative to the mean observed CO.
[d]Standard error of mean bias (Δ).
[e]R is the linear correlation coefficient between model and observations.
[f]R_{ds} is the linear correlation coefficient between deseasonalized model and observations.
[g]R_{dst} is the linear correlation coefficient between deseasonalized and detrended model and observations.
[h]The annual trend is given in %/a ± two standard errors.
[i]NOAA/GMD data for the site flagged as being "nonbackground" were not included.
[j]Data provided by Ernst Brunke and Eckhart Scheel [*Brunke et al.*, 1990].
[k]NS, not significant.

Table 12. Station Information for Observed CO Column Data With Statistical Comparison to Model Output

Station	Latitude, deg	Longitude, deg	Altitude Range, km	Time Period	N[a]	Δ[b]	Δ,[c] %	Standard Error[d]	R[2e]	R_{ds}^{2f}	R_{dst}^{2g}	Trend Model,[h] %/a	Trend Data,[h] %/a
Jungfraujoch	46.5°N	8.0°E	>3.6	88–99	100	NS[i]	NS	0.009	0.72	0.27	0.26	−0.8 ± 0.3	−0.6 ± 0.4
Rikubetsu	43.5°N	143.8°E	0.2–12	95–00	30	NS	NS	0.04	0.70	0.20	0.19	–	–
Mauna Loa	19.5°N	155.6°W	3.4–16	95–98	21	NS	NS	0.02	NS	NS	–	–	–
Lauder	45.0°S	169.7°E	>0.37	94–00	39	−0.064	−5.9	0.01	0.65	NS	0.12	–	–

[a]N is the number of measurement points coincident with model output.
[b]The bias ($\times 10^{18}$ molecules cm^{-2}) is the mean of (model-observed)/observed for the entire time series.
[c]Mean bias (%) relative to the mean observed CO.
[d]Standard error of mean bias (Δ).
[e]R is the linear correlation coefficient between model and observations.
[f]R_{ds} is the linear correlation coefficient between deseasonalized model and observations.
[g]R_{dst} is the linear correlation coefficient between deseasonalized and detrended model and observations.
[h]The annual trend is given in %/a ± two standard errors.
[i]NS, not significant.

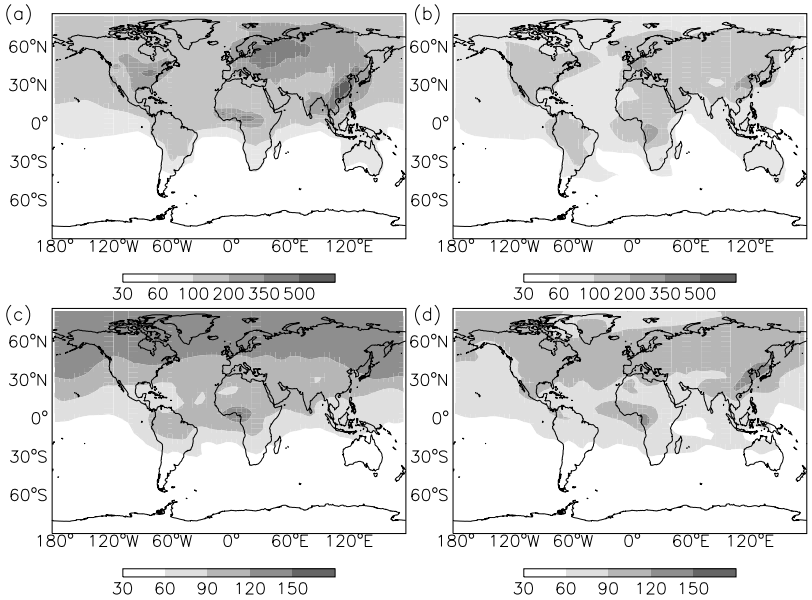

Figure 3. Model CO (ppbv) for 1994 at the surface in (a) January and (b) July and at sigma level 9 (~500 mbar) in (c) January and (d) July.

matter. The yield of CO from methanol oxidation is about 1 since CH_2O is the longest-lived intermediate species in the oxidation process (see section 3.5). We include a biogenic methanol source of 43 Tg C/a distributed according to emissions of isoprene; this results in production of 95–103 Tg CO/a (Table 1). Primary acetone emissions from biogenic sources are about 16 Tg C/a [*Jacob et al.*, 2002]. The yield of CO from its oxidation is assumed to be 0.66 on the basis of degradation pathways given by *Orlando et al.* [2000] and *Reissell et al.* [1999], resulting in a source of ~21 Tg/a (Table 1), which is distributed following *Jacob et al.* [2002].

4. Observations Used for Model Evaluation

[62] Model results were evaluated with observations from the NOAA/GMD surface network, various aircraft campaigns, total column stations, and from the space shuttle.

4.1. NOAA/GMD Flask Sampling Program

[63] Carbon monoxide is measured weekly at a global network of surface sites as part of the NOAA/GMD flask sampling program [*Novelli et al.*, 1992, 1998]. The stations

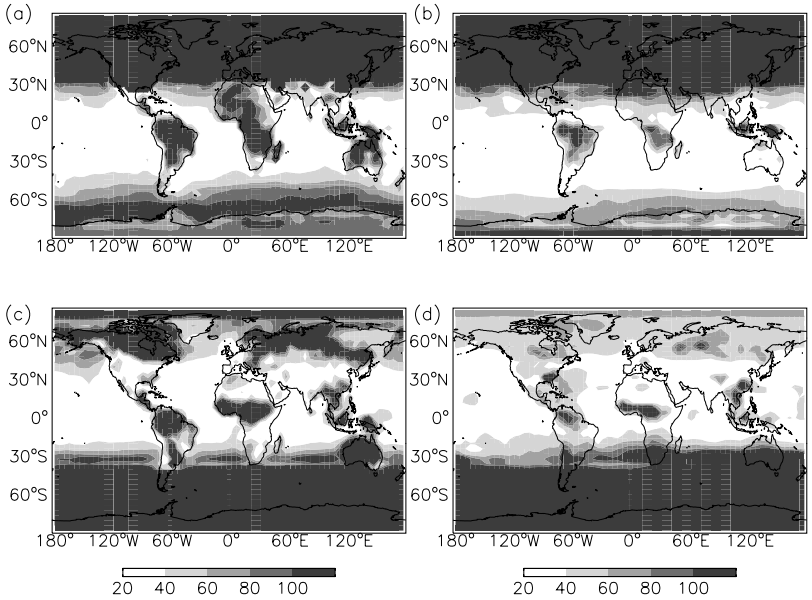

Figure 4. Lifetime of CO (days) at (a) the surface in January 1994, (b) ~500 mbar (sigma level 9) in January, (c) the surface in July, and (d) ~500 mbar in July.

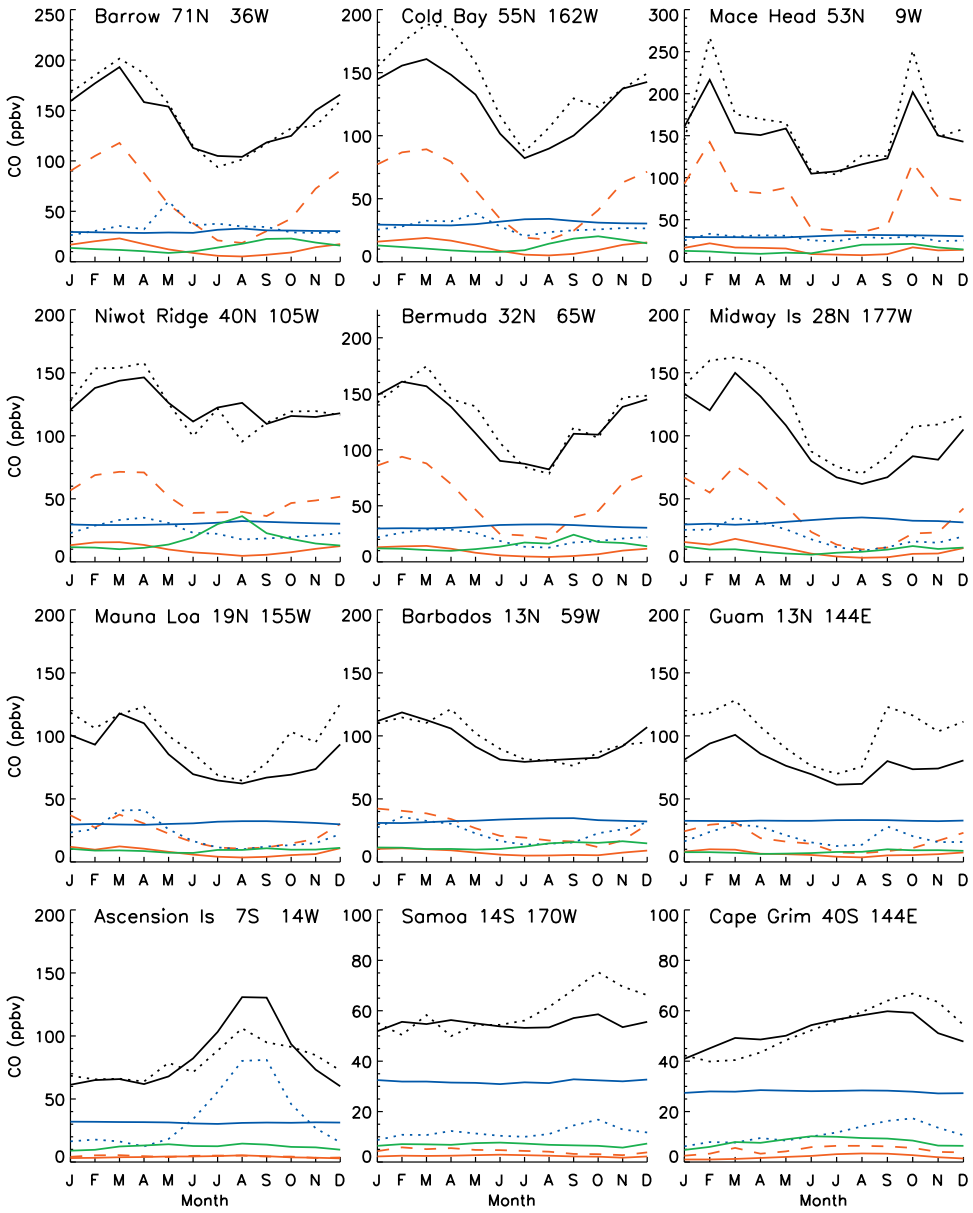

Figure 5. Contribution by source to model CO for 1994. The dotted black line represents NOAA/GMD CO observations for 1994, and total model CO is represented by a solid black line. CO from fossil fuels, biofuels, and biomass burning are shown as dashed red line, solid red line, and dotted blue line, respectively. CO from CH_4 oxidation is shown as a solid blue line and from biogenic NMHC as a solid green line.

used in this analysis are given in Table 11; they were selected because of their longer records. Data for Cape Point, South Africa, are continuous and from *Brunke et al.* [1990].

[64] As part of the GMD data selection, flask pairs are flagged as nonbackground if they deviate by more than 3 sigma from a smooth curve fit to the data. We include these data points, as long as they are duplicated, because we do not screen for nonbackground air in our model. We calculated monthly means from the weekly means. For Guam and Ascension Island, we show monthly CO calculated only with data for background conditions because of obvious contamination of the sampled air with CO from local sources on some occasions. We also use background data only for GMD shipboard data. Several surface sites employ a protocol to sample clean air, e.g., onshore winds for island and coastal sites. We did not account for selective wind sampling in the model. However, we sample from an adjacent grid box for locations with continental emissions within the box containing the site. These include the box to the south for Tae-ahn and the box to the southwest for Cape Grim and Cape Point. We also sample model output above the surface level for stations located at high elevation on mountain peaks: Niwot Ridge (level 5), Mount Waliguan (level 3), Tenerife (level 5), and Mauna Loa (level 7). We sample Grifton, located on a radio tower, at level 2.

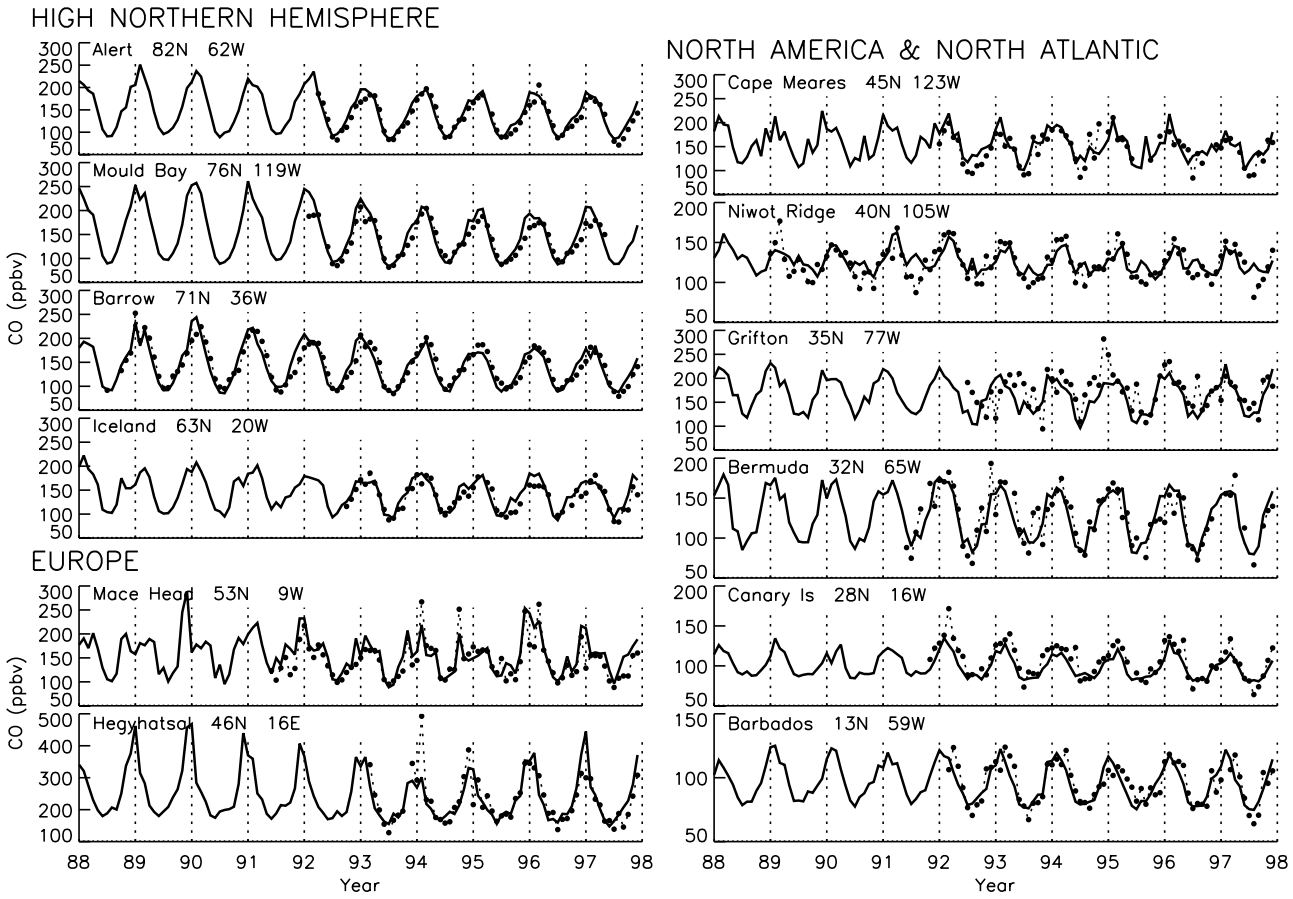

Figure 6. Time series of model surface CO with observations from the NOAA/GMD measurement stations. The model CO is represented by a heavy solid line, and the observations are represented by a dashed line with circles. Station locations are in Table 11. For the Guam and Ascension Island stations, the fine solid line represents the monthly averaged CO without data flagged as "nonbackground."

4.2. Aircraft Campaigns

[65] Observations from various aircraft campaigns were averaged over the same chemically and geographically coherent regions as described by *Bey et al.* [2001a]. Comparisons of vertical profiles of monthly averaged observed and model CO shown below use mean values for the same month and year that the field missions took place. These observations are not statistically representative for the particular month, but give useful information on vertical gradients in different regions and seasons.

4.3. Column Measurements

[66] We use column abundances of CO to evaluate the model at the following locations (see Table 12): Jungfraujoch, Switzerland [*Mahieu et al.*, 1997; *Rinsland et al.*, 2000]; Rikubetsu and Moshiri, Japan [*Zhao et al.*, 1997, 2000]; Mauna Loa, Hawaii, U.S. [*Rinsland et al.*, 1999]; and Lauder, New Zealand [*Rinsland et al.*, 1998]. The number of daily observations used to create the monthly averages typically ranged from 3 to 20.

4.4. Measurement of Air Pollution From Satellites (MAPS)

[67] Column measurements of CO were made from the space shuttle from 9 to 19 April and 30 September to 11 October 1994 [*Connors et al.*, 1999]. The instrument is most sensitive between 600 and 200 hPa. Connors et al. reported that the MAPS data agreed with in situ observations within ±10% while *Reichle et al.* [1999] found that the data are biased high by ~10%. We use the MAPS 5° × 5° interpolated, mission-averaged data product and compare to the average model CO for the same time period, after it is vertically integrated and weighted following Reichle et al.

5. Model Results and Evaluation

[68] Figure 3 shows model CO for January and July 1994, at the surface and at ~500 hPa. In January, there is a strong latitudinal gradient at both levels. The lifetime is long in winter, allowing CO from fossil fuel/industry to accumulate in the NH. Conversely, in the SH, CO approaches its seasonal minimum because its lifetime is short in austral summer (Figure 4) and biomass burning activities are at a minimum. By July, the latitudinal gradient is weaker because the CO lifetime is shorter (~weeks to months) over most of the NH, the biomass burning season is beginning in the SH, and the lifetime is long at southern midlatitudes.

[69] There are strong surface gradients near the industrialized regions of North America, Europe, and east Asia in January, and regions with biomass burning, especially northern Africa in January and southern Africa in July. There are also gradients at 500 hPa over regions with

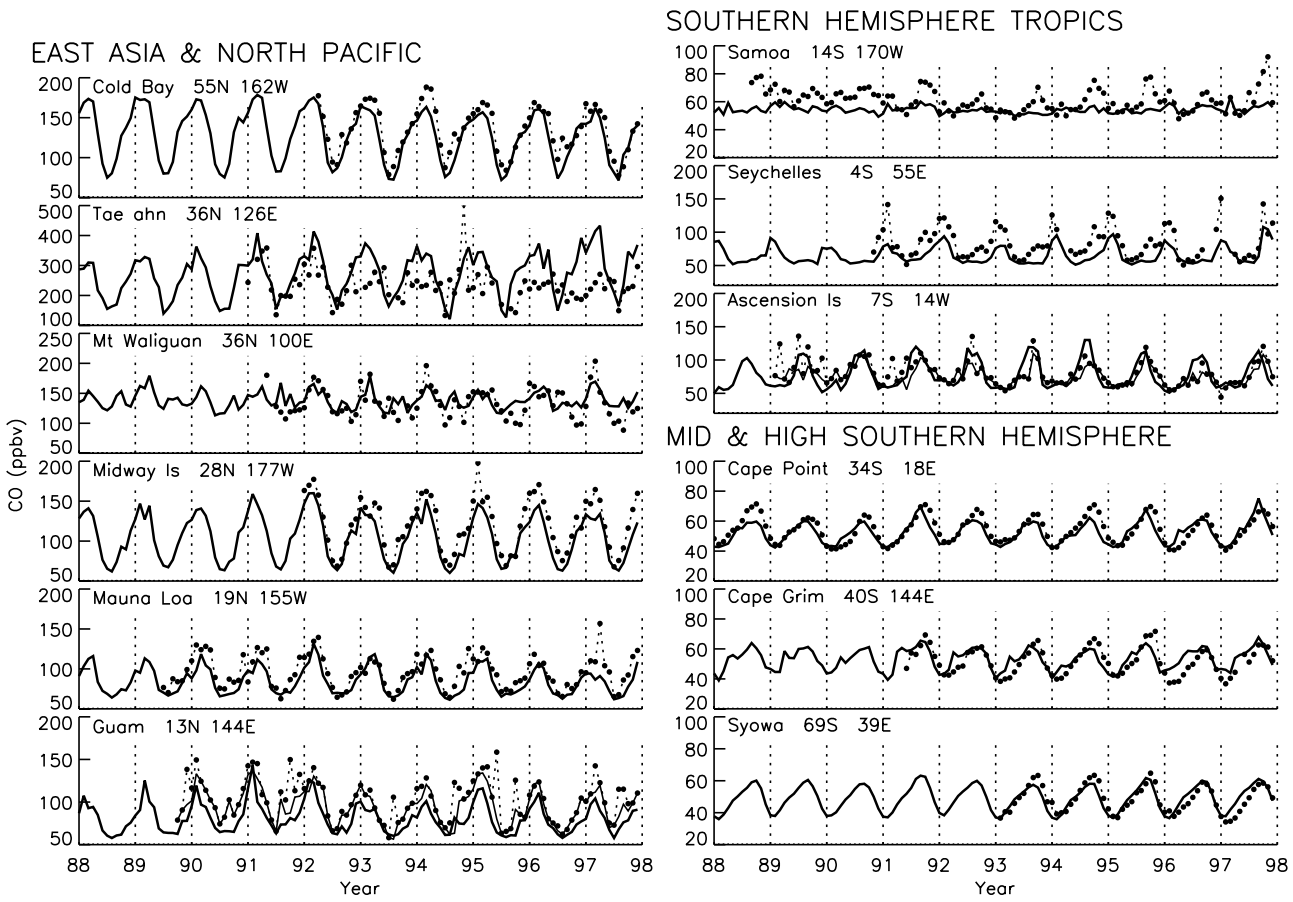

Figure 6. (continued)

biomass burning, indicating that vertical transport in these tropical regions is important for pollutant dispersion. On the other hand, CO at 500 hPa in January is well mixed in the NH extratropics, as horizontal advection in the prevailing westerlies is the dominant mechanism for mixing.

5.1. Source Apportionment

[70] The contribution of various sources to surface CO is shown for selected sites in Figure 5. These contributions were calculated using tagged CO tracers [*Bey et al.*, 2001b] for each source and monthly mean OH fields from our simulation with all sources. The apportionment of sources in our model is similar to the apportionment in the model of *Holloway et al.* [2000]. Methane oxidation contributes 25–30 ppb CO everywhere, year-round. Fossil fuel emissions are the largest contributor to the CO burden in the northern extratropics. Our model's burden from fossil fuels is up to 50% larger than that reported by *Holloway et al.* [2000], because they used a smaller fossil fuel source. The seasonal contribution from biomass burning at the tropical stations is generally equal to or less than that from CH_4 oxidation (Figure 5). *Holloway et al.* [2000] found the reverse, because of higher emissions in their work. The contribution of biogenic NMHC at all stations is less than that reported by *Holloway et al.* [2000] as a result of higher emissions in their work (Table 1).

5.2. Time Series (1988–1997)

[71] We present here an evaluation of the model (Figures 6 and 7). Our goals are (1) to test the emission inventories used here, (2) to show the ability of the model to reproduce observed CO, and (3) to quantify the ability of the model to reproduce CO trends and IAV. We show the trends here, and focus on their causes in the work by Duncan and Logan (manuscript in preparation, 2007). In what follows we give a brief overview of our results and then discuss our findings by region.

[72] Several quantitative measures of model performance are given: the bias, the correlation coefficient between simulated and observed time series (R), and the trend. Since a large part of the correlation is driven by the model's ability to capture the seasonal cycle of CO, we use the correlation for the deseasonalized time series (R_{ds}) to quantify IAV; and since there are significant trends at several sites, we use deseasonalized and detrended time series (R_{dst}) to indicate the model's ability to capture the residual IAV that is not caused by trends. Seasonal trends were calculated using linear regression as described in Appendix A. We focus below on trends at sites with longer records; for short records, the trends can easily be skewed by a few outliers.

5.2.1. Overview

[73] There are no consistent regional biases in the extratropics, and biases are mostly less than ±10% in the NH and ±5% in the SH (Table 11). However, model CO is low at many tropical sites with biases of zero to −19%. The model captures well the phase and amplitude of the seasonal variation of CO. Model and observed CO are highly correlated, with $R^2 > 0.5$ for 80% of sites, and >0.7 for half.

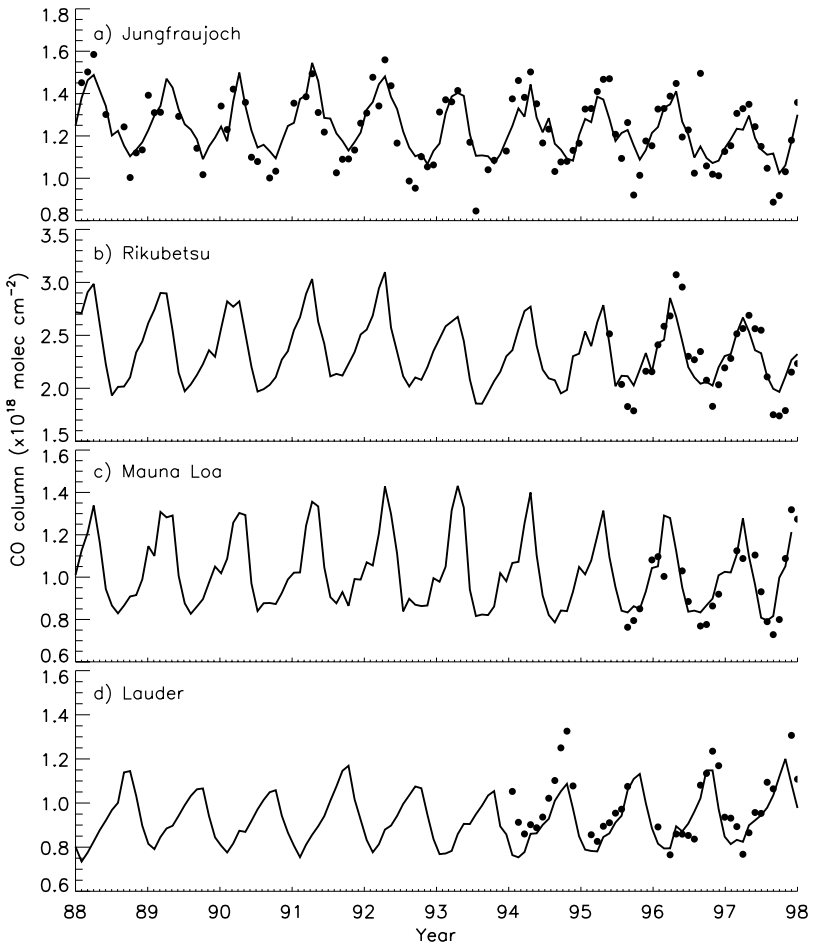

Figure 7. Comparison of observed (dots) and total model columns (line) of CO ($\times 10^{18}$ molecules cm^{-2}) for (a) Jungfraujoch, (b) Rikubetsu, (c) Mauna Loa, and (d) Lauder. Station locations are in Table 12.

[74] The simulation captures well the observed decrease in CO at northern high latitudes (−2%/a for 1988–1997) and over the subtropical Pacific (−1%/a for 1989–1997), but underestimates the decrease over the Atlantic (approximately −2%/a for 1991–1997), as discussed further below. The model explains a significant fraction of the variance in the deseasonalized time series for most stations, with R^2_{ds} in the range 5–49%; the highest values are generally for stations with a significant decrease in observed CO. Once the trend is removed, the model explains a smaller (but significant) fraction of the variance at these stations (R_{dst} in Table 11).

5.2.2. High Northern Hemisphere

[75] Fossil fuels/industry provides the dominant source of CO in this region (Figure 5), and the model captures the decrease in CO that is associated with the decline in these emissions outside Asia, particularly in Europe [*Duncan and Bey*, 2004; Duncan and Logan, manuscript in preparation, 2007]. The mean model bias is small, ∼5%, and tends to be largest in winter. This may be caused by our scaling of the direct emission of CO from fossil fuels and biofuels by 1.19 to account for CO from the oxidation of coemitted NMHC, which in reality are long-lived in winter (section 3.6.1).

5.2.3. Europe

[76] Mace Head, on the west coast of Ireland, is influenced by relatively clean oceanic air and polluted air from Europe [*Simmonds et al.*, 1997; *Cape et al.*, 2000]. The model matches the transport-induced variability well, with R^2_{dst} = 0.47 [see also *Allen et al.*, 1996a]. This variability is partly associated with the North Atlantic Oscillation (NAO) [*Duncan and Bey*, 2004]. The strong emissions reduction in Eastern Europe and Russia is not apparent at Mace Head because these emissions are generally downwind and the meteorological variability effectively masks the impact of the emissions reduction [*Duncan and Bey*, 2004]. However, there is a small decrease in column CO over Switzerland (−0.6%/a at Jungfraujoch), also found in the model.

[77] Hegyhatsal (Hungary) is a regionally polluted site with CO values 2–3 times higher than at remote sites. The model captures the IAV there (R^2_{dst} = 32%), as it does for the column measurements at Jungfraujoch (R^2_{dst} = 25%). The model and observed trends at Hegyhatsal are of opposite signs for 1993–1997, the time when data are available, because of a low bias in the winter of 1993–1994 and a high bias in the winter of 1996–1997. The IAV at this site effectively masks the 15–20% decrease in emissions in Western Europe during this time.

[78] European fossil fuel use provides the largest source of CO to the European and high-latitude sites. This source generally contributes more than 40% to the total burden [*Duncan and Bey*, 2004] and even more when the contri-

bution from methane oxidation (~20–25 ppbv) is removed. The good agreement between the model and observations suggests that errors in our estimate for this European source are relatively small.

5.2.4. North America and North Atlantic

[79] Model CO is a few percent higher than observations at most U.S. stations, including those with shorter records not shown in Figure 6 (in Wisconsin and Utah). We do not reproduce sampling protocols at Cape Meares, Oregon and Niwot Ridge, Colorado (westerly winds for both), which may explain the relatively low values for R^2 (0.62, 0.51). The model does not reproduce CO well at Grifton, North Carolina, with a negative bias of −6% and R^2 = 0.29. The model may perform poorly there because it does not simulate local pollution episodes well.

[80] The model performs well at the North Atlantic stations, with no bias for Bermuda or Barbados and a bias of −6% for the Canary Islands. All three sites show a decrease in CO for their short records (~6 a). The model underestimates the trends, but is within the error bounds except for the Canary Islands. It captures the IAV well at the latter site, with R^2_{ds} = 0.31; some of the IAV in model CO may be associated with the NAO as the CO burden from European sources tends to be higher over the North Atlantic when the NAO is in the negative phase, and lower when it is in the positive phase [*Duncan and Bey*, 2004]. Fossil fuels from North America provide the largest source of CO at the U.S. sites and at Bermuda (40–50% when the source from CH_4 oxidation is excluded), and the small biases lend support to the inventory for North American emissions.

5.2.5. East Asia and North Pacific

[81] Tae-ahn, Korea, lies in a region of high fossil fuel emissions. The model is much too high in winter and spring, when Asian outflow is at a maximum, but the station data are sampled to avoid such outflow, likely causing the high bias (23%) and low R^2, 0.17. The CO column over Rikubetsu, Japan, has no bias (Table 12). Mount Waliguan is in a region with a strong gradient in Asian fossil fuel emissions. The model is too high in late summer and fall, causing the small bias (6%) and a relatively low value for R^2, 0.39.

[82] The model is low (approximately −11%) for the Pacific sites of Cold Bay, Midway, and Mauna Loa, particularly in January–March when the contribution from fossil fuels is highest (Figure 5); however there is no bias for the CO column above Mauna Loa (Table 12). The model matches the decrease in CO for the longer records, −1%/a, caused by the decrease in European emissions (Duncan and Logan, manuscript in preparation, 2007). Fossil fuel emissions (from Europe, Asia, and North America) and biomass burning are the largest CO sources for these sites (Figure 5). The negative biases suggest that emissions from east Asia are somewhat underestimated, as there is no indication that European and North American emissions are low. There are also low biases in shipboard data from the eastern Pacific in spring from 10–30°N (Figure 8a). However, there are high biases for shipboard data near southern Asia for 18–21°N in spring when outliers are excluded, but not when they are included (Figure 8b).

[83] The model underestimates CO at low latitudes in the Pacific as shown by the shipboard data (Figure 8) and results for Guam; here also the biases are largest in winter and spring, except for the south China Sea, where the biases are largest in August to October. There appear to be local sources on Guam, and the bias for background data there is −13%. The model reproduces the small decrease in CO, −1%/a.

5.2.6. Southern Hemisphere Tropics

[84] The model performs best at Ascension Island, the site most sensitive to emissions from fires (Figure 5), with no bias but a relatively low R^2 (0.42). The model results are slightly better when only background data are used. Weekly measurements are unlikely to capture the true variability for this location, which is caused by mixing of more polluted air from above. Aircraft measurements show a highly layered structure, with values above the boundary layer much greater than those below [*Talbot et al.*, 1996]. The observations show a decrease in CO, −2.3%/a, while the model gives no trend; biomass burning emissions are the same each year in Africa in the model, as their IAV could not be determined reliably [*Duncan et al.*, 2003a].

[85] The model performs poorly at Samoa. It does not capture the seasonal cycle (Figure 5, R^2 = 0.27) and is biased low by 10%. Samoa is located near the South Pacific Convergence Zone (SPCZ) [*Merrill*, 1989], and the data show considerably variability in austral spring. Aircraft measurements for this season show that CO is much higher south of the SPCZ than to the north, because of transport of emissions from fires in Africa and South America in the subtropics [*Gregory et al.*, 1999]. *Allen et al.* [1997] reported that the spatial extent of deep convective mixing is overestimated in the model from June to August in the vicinity of the SPCZ, and Samoa is in a region of deep convective mixing in the model. This acts to reduce the variability and concentration of CO in the boundary layer.

[86] The model also performs poorly at the Seychelles, in the Indian Ocean, with a bias of −19%; it is too low by up to 40 ppb in January–February, the seasonal maximum. At this time of year the station is effectively in the NH, with the ITCZ to the south, allowing it to be affected by pollution from south Asia [*Lelieveld et al.*, 2001]. A recent assessment of CO from mobile sources in India indicates that kerosene provides a significant source [*Dickerson et al.*, 2002], not accounted for in the inventory used here. The Seychelles may also be influenced by emissions from northern biomass burning, but the model transports less than 5 ppb of this source to the site. The data show a secondary maximum in September–October during the SH biomass burning season, particularly in 1991, 1994, and 1997, when the site is influenced by emissions from fires in Indonesia [*Duncan et al.*, 2003a, 2003b]; the contribution is less than 10 ppbv except in 1997, when there were unusually intense fires. The maximum is caused by transport of emissions from fires from N. Africa and S.E. Asia, and from fossil and biofuel use in south Asia. The model simulates the timing of this peak quite well, but not the magnitude. It captures much of the IAV, with R^2_{ds} = 0.4. The model simulates the transport from different source regions and its variability rather well.

[87] The tropical sites alone do not offer strong constraints on biomass burning emissions, because of transport issues for Samoa, and the complexity of sources for the Seychelles. Ascension is the site most sensitive to these emissions, and does not imply an error in their magnitude.

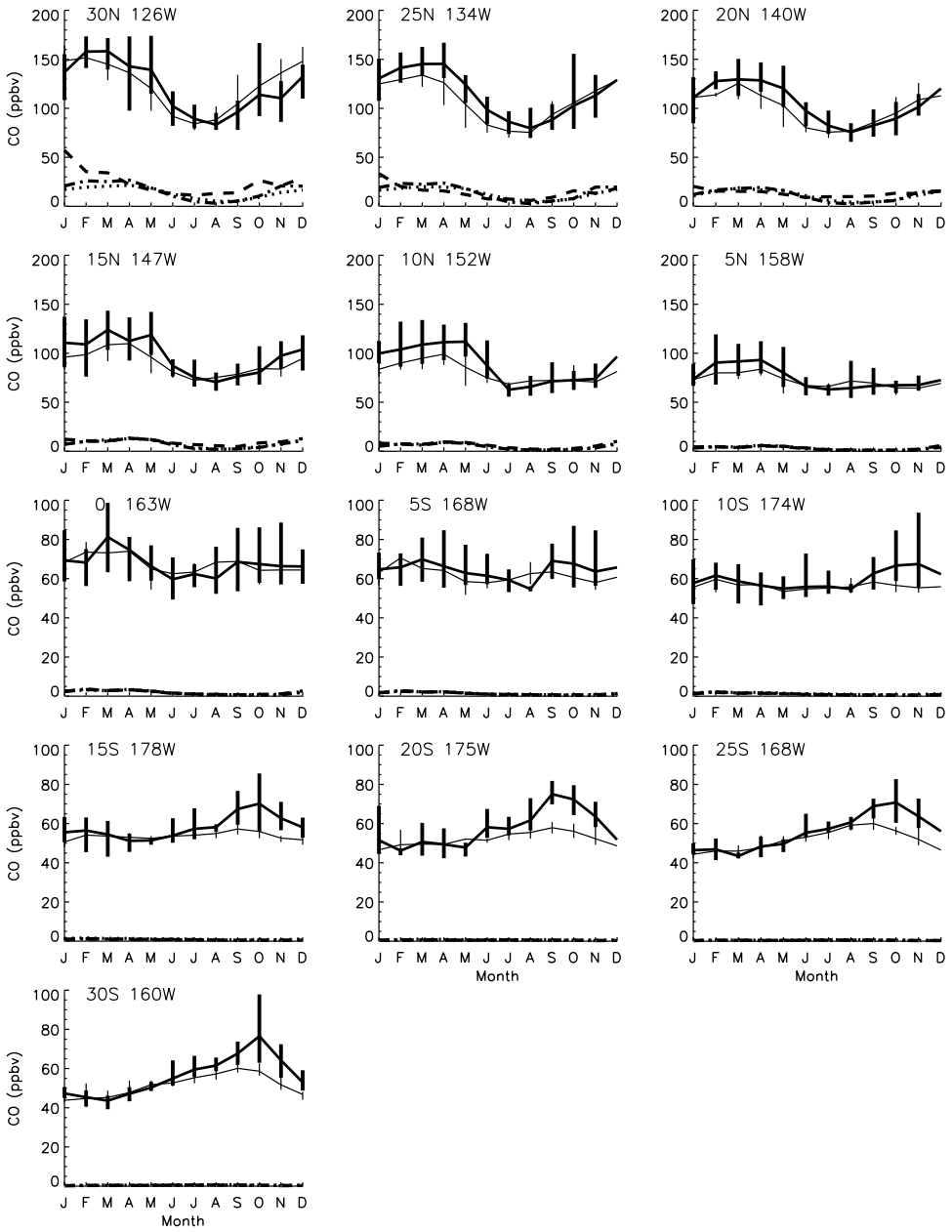

Figure 8a. Comparison of model CO (thin line) with shipboard observations (thick line) in the Pacific Ocean. The model CO is averaged over the time period of the observations. Model CO from North American, Asian, and European fossil fuel sources is shown as dashed, dotted and dashed-dotted lines, respectively. The vertical bars show the maximum and minimum values of model CO (fine line) and observations (thick line). The observations do not include data marked as outliers.

However, the shipboard data from the tropical Pacific show a strong underestimate in austral spring (Figure 8a), which must result either from low emissions from fires or from deficiencies in transport.

5.2.7. Middle and High Southern Hemisphere

[88] There are only small biases for the stations in this region, −3% to 5%, and for the column over Lauder, −6%. However, the model is usually low in August to November, the season when transport of biomass burning emissions is an important source (Figure 5). The model peaks about one month early. This could be caused by the biomass burning season ending too early, but this seems unlikely as the timing of fires is based on satellite observations [*Duncan et al.*, 2003a]. The enhanced CO in the model in fall at Cape Grim is from fires in Australia, but samples are collected in marine air. We removed Australian sources, and improved significantly the model in austral fall (not shown). There are small downward trends at Cape Grim (−0.8%/a) and Cape Point (−0.37%/a) that are not seen in the model.

[89] The underestimate of the seasonal maximum in the southern extratropics, coupled with the Pacific ship data, further supports the idea that the emissions from biomass burning may be too low in the SH and/or there are deficiencies in transport.

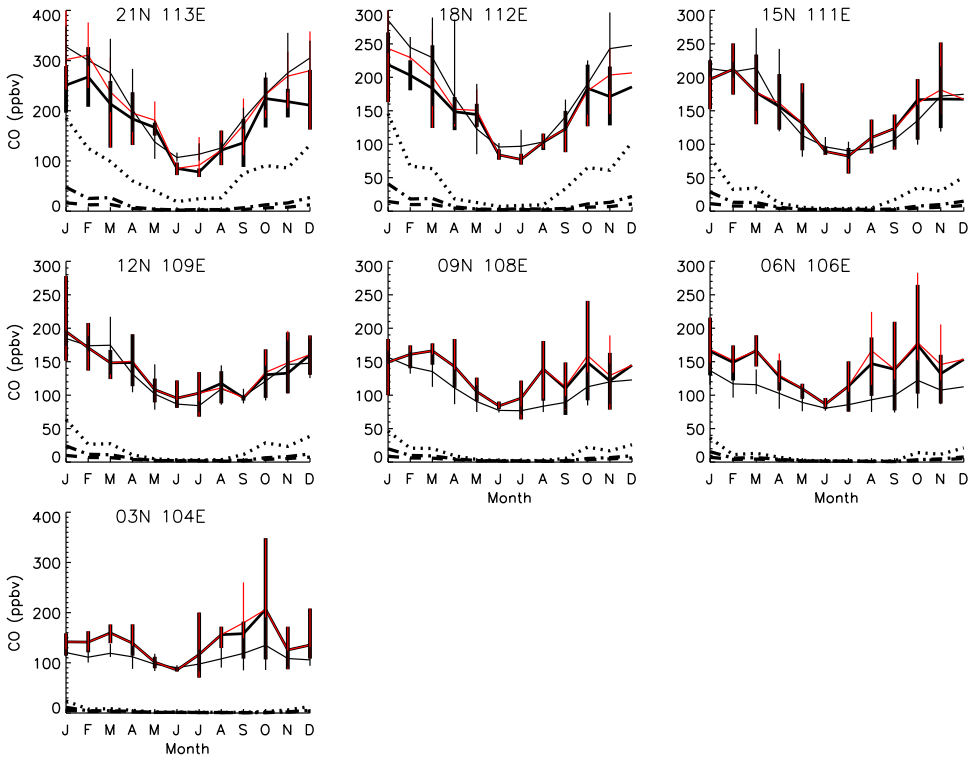

Figure 8b. Same as Figure 8a except for shipboard data from the South China Sea. The red line represents the monthly averaged observations when outliers are included.

5.3. Aircraft Campaigns

[90] Model results compare well with observations for most regions, capturing the lack of vertical gradient in the tropics and SH (except near sources) and the decrease with altitude in the more polluted northern locations (Figure 9). The model is within the range of the data for North America, except it is biased low over Maine above the boundary layer. However, it is systematically high immediately downwind of Asia, on the basis of data from 1991 and 1994. The model agrees well with the data from the southern tropical Atlantic and Pacific during the biomass burning season (September 1992 and 1994). The outflow of CO from Africa to the Atlantic is too low in altitude, but is of about the right magnitude.

5.4. Space-Based Data

[91] The MAPS data provided the first global pictures (albeit brief) of CO [*Reichle et al.*, 1999]. The model reproduces well the strong gradient with latitude and the relatively small gradient with longitude in April 1994 (not shown), with no global bias and $R^2 = 0.87$. However, model CO is slightly high in the NH, and low at southern midlatitudes, where it is less variable than the observations.

[92] The model is systematically low in October 1994 in the southern tropics (Figure 10) where biomass burning is occurring, especially in areas typically influenced by outflow from Indonesia (i.e., the tropical Indian Ocean and Africa, the regions of the subtropical jets over the Pacific Ocean [*Duncan et al.*, 2003b]). This implies that the emissions from biomass burning are too low, particularly those from Indonesia. The model uses monthly mean emissions, so it cannot reproduce transport of CO from specific fires seen by MAPS on its ~10 d in orbit, possibly giving rise to the low correlation between model and observations. The low bias in October is also consistent with the comparisons with SH surface data in October 1994 (Figure 6).

6. Sensitivity Studies

[93] Here we examine the sensitivity of CO to uncertainties in OH and to emissions. We are motivated by the patterns revealed in the model evaluation: biases at 11 northern extratropical sites of −9% to 8%, with a mean bias of 2% (excluding Tae-Ahn), either zero or negative biases in the tropics, and small biases in the southern extratropics. Since the model underestimates CO in much of the tropics even though our lifetime for CH_3CCl_3 is reasonable (section 2), we conducted a simulation with archived OH values decreased by 20%. The EDGAR estimate for the source of CO from fossil fuels and industry is about 25% smaller than that used here (Table 9), and we ran simulations with this source changed by ±25% (±25% FF below). There are larger uncertainties in sources from biomass burning and biogenic NMHC, so we ran simulations with these sources changed by ±50% (±50% BB and ±50% BIO below). Figure 11 shows the results of our sensitivity simulations for selected stations. Detailed results, including results for more stations (Figures S1–S3[1]) and the mean biases for the surface stations, are given in the auxiliary material.

[1]Auxiliary materials are available in the HTML. doi:10.1029/2007JD008459.

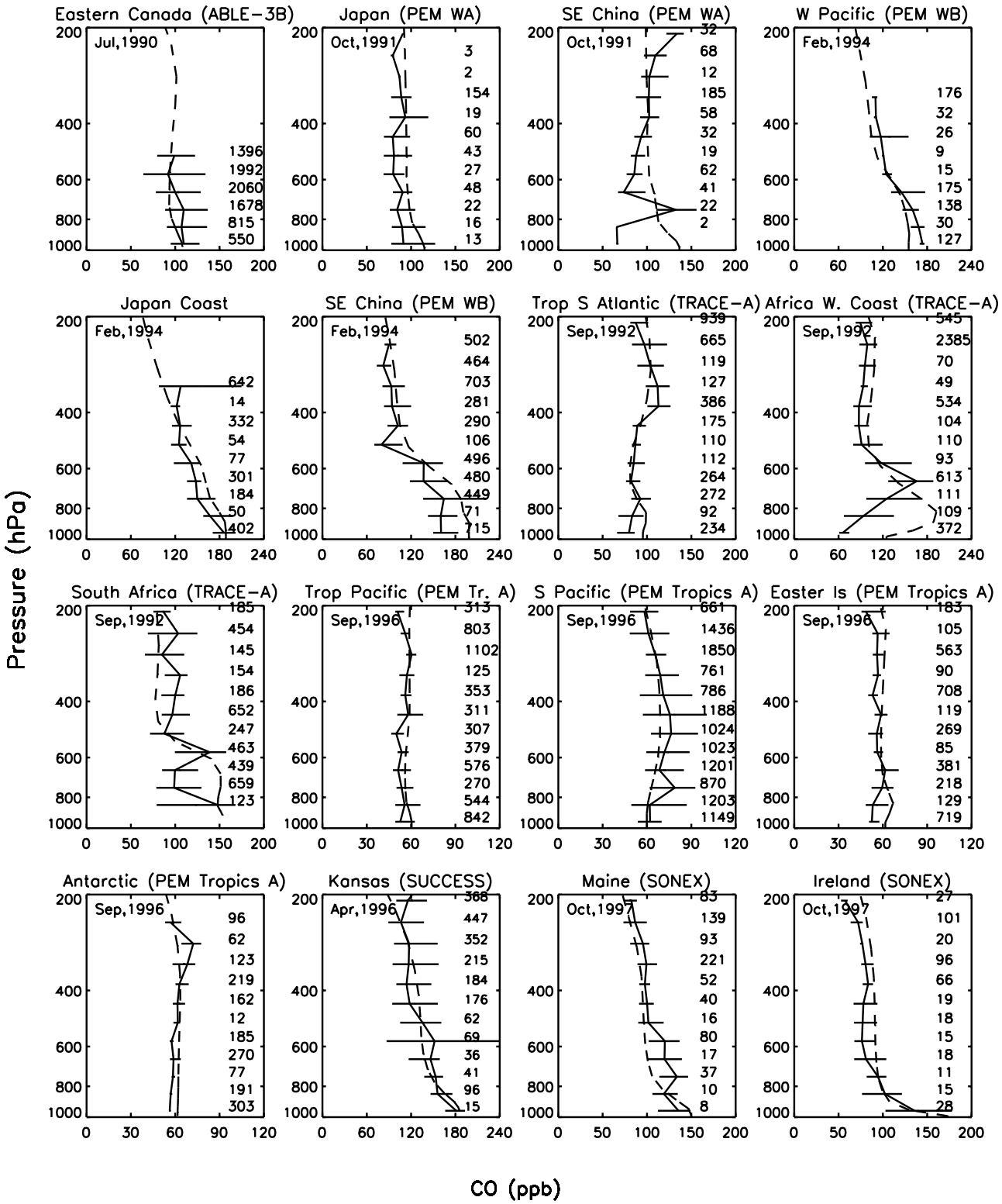

Figure 9. Comparison of observed (solid line) and simulated (dashed line) vertical profiles of CO. The horizontal bars are the standard deviations of the observed values.

6.1. Lower Tropospheric OH

[94] Lower OH improves agreement between model and observations in regions where the model is biased low, the Pacific from 30°N to 15°S, and the Seychelles (Figures 11a and S1). Conversely, lower OH degrades the model results in the tropical and subtropical Atlantic, and in the extratropics. The model fails to capture the seasonal maximum of CO in the southern tropical Pacific (Samoa, and shipboard data in Figure 8a), and underestimates the seasonal maximum in the northern Pacific (Cold Bay, Midway and Mauna

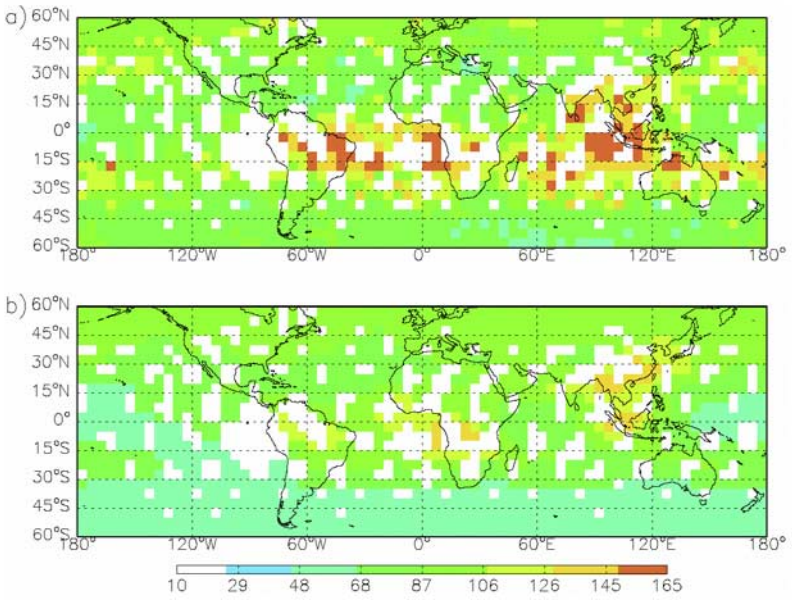

Figure 10. (a) MAPS CO (ppbv) at ~500 mbar observed from the space shuttle in October 1994 and (b) model CO.

Loa). These deficiencies are likely caused by problems with sources or transport in the model, rather than by an overestimate of tropical OH.

6.2. Fossil Fuels

[95] The base case gives the best agreement for stations in North America, Europe, and the north Atlantic (Figures 11b and S2). For the high latitudes the biases are also smallest for the base case, but because the phase of the model's annual cycle is about a month early, the +25% FF case agrees best in April to June, while the −25% FF case does in August–December. The higher emissions improve the overall biases in the Pacific from 55°N to 13°N. Emissions from Europe and Asia contribute significantly to CO over the north Pacific, so to reconcile the results for the entire Pacific could require an increase in Asian emissions and a decrease in European emissions. Some of the difficulties in matching the seasonality of CO in the extratropics may be caused by (1) our assumption that NMHC coemitted with CO are an immediate source of CO, even in winter, while in reality the NHMC are long-lived in winter (section 3.6.1), and (2) an underestimate in the seasonality in emissions from fossil fuel, as we did not allow for seasonality in the residential sector (section 3.1.1).

[96] Where fossil fuels provide the largest source (north of ~30°N), higher emissions increase CO by ~14%, while lower emissions decrease it by ~14%, with largest effects closest to source regions. The +25% FF case improves the model biases by 6–10% in the northern tropics, but has little effect in the SH. The effect of a 25% increase in fossil fuel emissions is somewhat smaller than that of a 20% decrease in OH at remote locations in the northern extratropics while the converse is true near source regions. Our results imply that our estimates of global CO emissions from fossil fuels and industry are unlikely to be in error by as much as +25%, unless our OH concentrations are too high.

6.3. Biomass Burning

[97] Increasing biomass burning emissions by 50% improves model CO at almost all tropical and subtropical stations in local spring, except Ascension (Figures 11c and S3). Ascension Island is the site most sensitive to fire emissions and for most other tropical locations, biomass burning provides at most 25–30% of CO. However, higher emissions degrade the simulation in the southern extratropics, except in October–December. Transport of emissions from fire to the extratropics provides about 25% of the CO there in the burning season. The effect of a 50% increase in emissions is similar to that of a 20% decrease in OH in the tropics and the SH, except near source regions.

[98] In the northern extratropics, where fires are a minor source of CO except for boreal regions in May–August, the +50% BB case improves the simulation slightly where the base case has negative biases, while the −50% BB case worsens it where the base case has positive biases, with changes in the biases of only ±7%.

[99] Production of CO from biogenic NMHC oxidation, another large tropical source, is not likely the cause of the local spring underprediction as it does not have strong seasonal variation. Changing this source by ±50% has similar effects on model results at most stations to the ±50% BB cases as shown in Table S1, so results are not discussed further.

7. Discussion and Conclusions

[100] We presented a comprehensive discussion of the sources of CO, with a focus on uncertainties in the source from fossil fuels and industry, and tested our budget with a simulation of CO for 1988 to 1997 using a CO-only version of the GEOS-Chem model. Unlike previous studies, we simulated the interannual and seasonal variation of emissions of fossil fuels and biomass burning, and allowed for IAV in transport, the overhead ozone column, and methane.

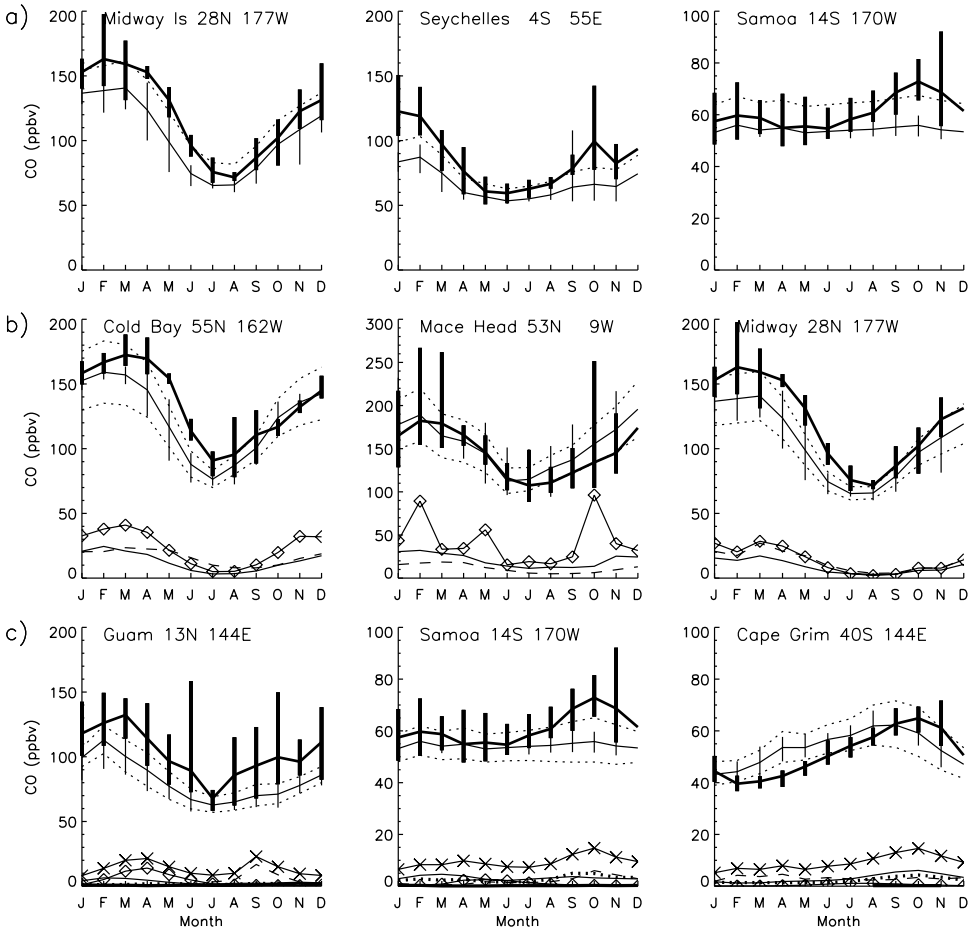

Figure 11. (a) Comparison of model CO and observations from the NOAA/GMD stations for the reduced OH sensitivity study. The model CO is averaged over the time period of the observations. The heavy solid line represents observations, and the vertical bars are the maximum and minimum measured values. The fine solid line with vertical bars represents the base simulation and the dotted line represents the simulation with archived OH reduced by 20%. (b) Same as Figure 11a except for fossil fuel adjusted by ±25% (dotted lines). The contribution of fossil fuel emissions to the burden for 1994 for the base simulation is shown for Europe (fine line with diamonds), North America (fine line), and Asia (dashed line). (c) Same as Figure 11b except for biomass burning adjusted by ±50% (dotted lines). The biomass burning contribution in the 1994 base simulation burden is shown for Asia (fine line with diamonds), Africa (fine line), boreal forests (heavy solid line), Indonesia and Australia (dashed line), and Latin America (dotted line). The total burden from biomass burning is shown as a fine line with crosses.

[101] The model was evaluated with observations from the NOAA/GMD surface sites, column measurements, aircraft profiles, and MAPS data from the space shuttle. The ability of the model to reproduce observations reasonably well offers constraints on our source estimates, and lends confidence in the use of the model as a tool to study interannual variations and trends in CO. The parameterized chemistry decreases significantly the model run time as compared to the simulations with a kinetic solver, and permits multiple decade-long sensitivity simulations. We evaluate the trends in CO here, and present a more detailed study of the causes of the trends and interannual variability in the work by Duncan and Logan (manuscript in preparation, 2007).

7.1. Emissions of CO and Their Uncertainties

[102] Our estimate for the source of CO from fossil fuels and industry is 390 Tg in 1985. North America and the FSU/Eastern Europe provide the largest sources, 28% and 25% respectively, and only 5% of emissions are in the SH. By scaling CO emissions to national inventories where available, and to liquid fuel consumption elsewhere, we estimate that the global source changed by only a few percent from 1985 to 1997. However, the source from eastern Asia increased by 51% from 1988 to 1997, driven by economic expansion, while that in Eastern Europe decreased by 45%, driven by economic contraction. There were smaller decreases in Western Europe, 32%, and North America, 17%, over the decade, as a result of regulation of vehicular emissions. Our approach may have overestimated the increase in China, but by only ~16 Tg in 10 a.

[103] Our estimate for the direct CO source from fossil fuels and industry in 1985, 390 Tg, is 30% larger than the EDGAR 2 estimate for 1990, 298 Tg, and larger also than the EDGAR 3.2 inventories, 319 Tg for 1990 and 310 Tg

for 1995. We find higher emissions for all sectors compared to EDGAR 2, but the difference results mainly from our estimate for industrial sources, and for coal combustion in the industrial sector, where we allowed for highly inefficient combustion in China.

[104] The EDGAR 2 and EDGAR 3.2 inventories have been used as the prior for the inversion analyses summarized in Table 2. In all cases, the forward models underestimated CO significantly in the northern extratropics, and the posterior emissions were significantly higher than the prior. Most inversion studies that derived regional emissions found that sources from Asia were seriously underestimated, by as much as a factor of two [*Kasibhatla et al.*, 2002; *Pétron et al.*, 2002, 2004; *Arellano et al.*, 2004, 2006]. In some studies, sources from North America and Europe required little adjustment, while in others the inversion implied smaller sources than the prior.

[105] The latest work by *Streets et al.* [2006], based on detailed Chinese statistics for fuel use by sector and new data on EFs from China, gives emissions for China in 2001 that are very similar to the total used here for 1997. Their detailed study is a major improvement over our crude estimate, but it confirms our supposition, made over a decade ago, that inefficient combustion in small-scale industrial units is a major source of CO in China, and that emissions from the iron and steel industry may be significantly underestimated in the developing world. It is likely that we underestimate emissions from industrial processes and small-scale combustion in other Asian countries such as India. As we emphasized in section 3.1.1, uncertainties remain in emissions of CO for the transport section in developed countries [*Sawyer et al.*, 2000; *Dickerson et al.*, 2002], with even larger uncertainties for developing countries.

[106] Inversion studies offer promise for constraining CO emissions estimates, but they are no panacea, as shown by the variable results in Table 2. Most inversions do not try to infer the source from fossil fuel/industry separately from the biofuel source, as they are colocated in Asia. We find good agreement with observations in the northern extratropics with a source from fossil fuels/industry and biofuels of 633–676 Tg/a; this includes CO from the oxidation of coemitted NMHC. The inversion studies infer a source of 760–923 Tg/a for this category, with the results depending in part on the model OH, in part on the dynamical model, and in part on the observations used as the constraint. For example, two GEOS-Chem based inversions (using the same OH distribution) give an estimate of 768 Tg/a with GMD data as the constraint, but 844–923 Tg/a with MOPITT data as the constraint (Table 2) [*Kasibhatla et al.*, 2002; *Arellano et al.*, 2004].

[107] The source of CO from photochemical oxidation of CH_4 and NMHC represents more than half of the total source of CO (Tables 1 and 2), larger than direct emissions from biomass burning, fossil fuels, and biofuels. The yield of CO from CH_4 oxidation is a potentially major source of uncertainty as CH_4 oxidation accounts for ~30% of the total CO source (Tables 1 and 2). We argue that the yield of CO is close to unity, in agreement with *Novelli et al.* [1999], because of the low solubility of key intermediate products, CH_2O and CH_3OOH. Others have argued that yields are as low as 0.7, based on analysis of CO isotopes [*Manning et al.*, 1997; *Bergamaschi et al.*, 2000b]. A simulation with a yield of 0.9 results in lower CO by <5 ppbv than our simulation with a yield of 1. If the yield is indeed less than 0.9, then our model CO would be too low in the tropics and SH.

[108] The most uncertain source of CO from NMHC oxidation is from biogenic emissions, isoprene and terpenes (~250 Tg, 15% of the total source in Table 1); inversion analyses give 175–507 Tg/a (Table 2), and offer little constraint. Our sensitivity simulations to biogenic NMHC also do not constrain the source used here, because of the paucity of tropical observations. Oxidation of methanol provides a nontrivial source of CO, ~100 Tg.

[109] We find that oxidation of anthropogenic NHMCs increases the source of CO from fossil fuel and industry by 19%, or 72–76 Tg in 1988–1997. It increases the source from biofuels by 19% also (30 Tg), and the source from biomass burning by 11% (45–57 Tg). Together, these anthropogenic sources represent about 5% of the total CO source (Table 1).

[110] Another uncertainty in the CO budgets in the literature is the direct emissions of CO from plants, degrading plant matter, and the ocean (Table 2). We argue that the source from the ocean is small on the basis of measurements and that emissions from vegetation are roughly balanced by soil consumption.

7.2. Evaluation of the CO Budget, Trends, and Interannual Variability for 1988–1997

[111] We used comparisons between the model and observations by region to evaluate the emission inventories and to identify potential shortcomings. Stations heavily influenced by fossil fuel emissions from North America and Europe compare well with observations, indicating that the inventories for these regions are likely reasonable. However, the model underestimates CO over the North Pacific, particularly at the seasonal maximum, where emissions from both Europe and Asia are important contributors. While this could suggest that Asian emissions are too low, the solution to this problem is likely more complex.

[112] Our sensitivity studies imply that our inventory for fossil fuel and industry is in error by less than ±25%, unless the model OH is also in error. Inevitably, uncertainties in OH translate into uncertainties in constraints on CO sources. The budget of CH_3CCl_3 provides a constraint on OH primarily in the lower tropical troposphere, rather than on midlatitude OH, the main sink region for this CO source. Bottom-up estimates have tended to underestimate, rather than overestimate emissions, by not accounting properly for sources from inefficient combustion and small-scale industry in developing countries. On the basis of this consideration, and on inversion studies, we argue that our estimate is unlikely to be too low.

[113] Our model reproduces the downward trend in CO at high northern latitudes, −2%/a from 1988 to 1997. The trend is caused primarily by the decrease in European emissions. We found that the burden of CO at high latitudes is more heavily influenced by the decrease in European emissions than by the similar increase in Asian emissions (Figure 2) because the former are emitted at higher latitudes than the latter. Poleward export of European pollution leads to wintertime accumulation [*Duncan and Bey*, 2004]. The average lifetime of CO emitted from Europe is longer than

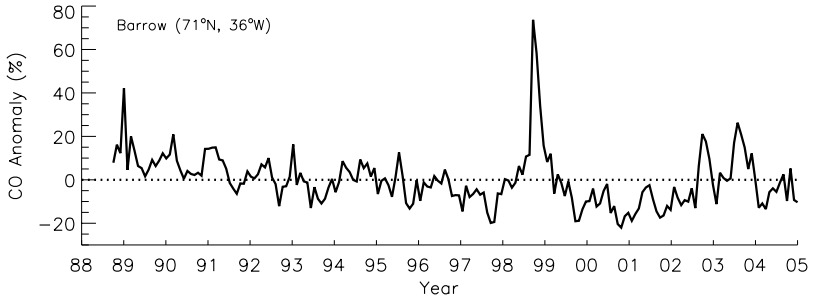

Figure 12. Observed monthly CO anomalies (%) at the GMD station, Barrow, Alaska, from 1988 to December 2004.

that from Asia, leading to a larger impact on high-latitude trends, as discussed further by Duncan and Logan (manuscript in preparation, 2007). There is also a downward trend in the northern Pacific, −1%/a from 1989 to 1997 that is captured by the model, and reflects the impact of the European source over this region.

[114] The IAV in CO in the northern extratropics has been linked to emissions from boreal fires, which occur between May and September [*Wotawa et al.*, 2001; *Novelli et al.*, 2003; *Yurganov et al.*, 2004, 2005; *Kasischke et al.*, 2005]. There were massive boreal fires in 1998, 2002, and 2003, primarily in Siberia, with emissions of 131, 118, and 90 Tg CO given by *Kasischke et al.* [2005]. Their estimates for emissions from boreal fires for 1992 and other years from 1995 to 2001 are <45 Tg/a. The CO record from Barrow, plotted as monthly anomalies in Figure 12, shows no evidence that boreal fires contributed significantly to the IAV in CO from 1989 to 1997, while the impact of the huge fires after our study period is clearly evident. There were also large boreal fires in May 1987 [*Cahoon et al.*, 1994] prior to the GMD measurements.

[115] The primary deficiency of the model is that it underestimates CO at the seasonal maximum in local spring in remote regions that are impacted by long-range transport of pollution: the tropics (excluding the Atlantic Ocean), the southern extratropics, and in the Pacific Ocean south of 55°N. This seasonal maximum results from transport of emissions from biomass burning and, in the northern extratropics, from the accumulation of CO during boreal winter, primarily from fossil fuels/industry, and the seasonality in OH removal. The agreement between model and observations is much better during the seasonal minimum where CH_4 oxidation provides half to two thirds of CO. The underestimate of the seasonal maximum may reflect the lack of seasonality of emissions from residential fuel use in the model, and this should be included in future inventories for CO, as was done for *Streets et al.* [2003] and *Wang et al.* [2005] for China.

[116] The model's underprediction in local spring in the tropics and SH may result from deficiencies in transport, an underestimate of emissions from tropical fires, and/or an overestimate of OH in the tropics. We showed above that a simple scaling of the OH fields does not solve this problem. Our comparison with MAPS data suggests that fire emissions were underestimated in October 1994, particularly in Indonesia.

[117] Emissions from tropical fires are frequently lofted by convection to the upper troposphere [e.g., *Pickering et al.*, 1996]. The frequency of tropical deep convective events is too high in the model [*Allen et al.*, 1997], a common problem for assimilated fields [e.g., *Wild et al.*, 2003; *Bloom et al.*, 2005]. *Allen et al.* [1997] showed also that the vertical extent of convection is too high over South America, and that GEOS-1 lofted fire emissions to higher altitudes than observed for a case study in September 1992. Consequently, the model's CO in the tropics may be excessively mixed in the vertical. If emissions are indeed lofted too high over Africa as well, they will be transported more effectively in the westerlies over the Indian and Pacific Oceans, where the excessively broad region of deep convection will vertically redistribute the CO; this will allow for faster removal in the lower troposphere, where OH is higher than in the upper troposphere. We note that although model CO is systematically low at the surface in August to December in the tropical south Pacific, the vertical profile in that region is reproduced reasonably well in September 1996 (Figure 9). Several other models, even when using posterior CO emissions from an inversion, fail to capture the magnitude of the seasonal maximum in the south tropical Pacific [*Bergamaschi et al.*, 2000a; *Müller and Stavrakou*, 2005; *Arellano et al.*, 2006].

[118] The sparseness of surface observations in the tropics makes it difficult to constrain satisfactorily the magnitude of the biomass burning source. Inverse analyses constrained by MOPITT data give a source of 410–580 Tg for 2000, similar to our bottom-up estimate of 450–570 Tg for 1988–1997 taken from *Duncan et al.* [2003a] (Tables 1 and 2). *Arellano et al.* [2006], using a later version of GEOS-Chem (with GEOS-3 meteorological fields), performed a seasonal inversion using MOPITT data; they found that the biomass burning emissions given by *Duncan et al.* [2003a] are too low in the southern tropics in September and October. Given the large uncertainty in bottom-up estimates of emissions from biomass burning, inversion analyses using satellite observations offer the most promise for constraining this source, but results depend on the model's dynamics and OH. *Arellano and Hess* [2006] show that the results of inversions are particularly sensitive to the treatment of convection and to transport out of the boundary layer in an intermodel comparison. Furthermore, inversion results using MOPITT data are not consistent with GMD surface data in the extratropical SH where biomass burning is a key source of CO [*Arellano and Hess*, 2006; P. Kasibhatla, personal communication, 2006].

Appendix A: Trend Analysis

[119] We compute the seasonal trends for simulated and observed CO for each station, and combined the seasonal trends to form the annual trend. We use the following linear regression model to calculate the trends from 1988 to 1997:

$$CO(t) = \sum_{i=1}^{12} m_i * I_i(month(t)) + \sum_{j=1}^{4} a_j * I_j(season(t)) + E(t) \quad \text{(A1)}$$

where m_i is the mean CO mixing ratio in month i, $i = 1, \ldots 12$; $CO(t)$ is the simulated CO in ppb as a function of time, t, in months; I_i is an indicator series for month i of the year which is equal to one if it corresponds to month i of the year and zero otherwise; a_j is the trend in ppb/a for season j; I_j is the indicator series for season, j; and $E(t)$ is the error term. The model includes 12 monthly means and four seasonal trends. The monthly means are weighted by the inverse of the interannual monthly variance. The variances are computed with two iterations after fitting the model, to remove the variation due to the trend. The annual trend is taken as the average of the four seasonal trends. The covariance matrix of the seasonal trends is used to calculate the standard error of the year-round trend. A trend is deemed statistically significant to 95% confidence levels if the absolute value of the trend is greater than two standard errors.

[120] **Acknowledgments.** We wish to thank Amanda C. Staudt for her work with emission factors, Andrew C. Fusco for processing TOMS ozone column data, Dylan B. Jones for providing us with stratospheric CO production and destruction rates, and Daniel Jacob for his methanol emissions. We also wish to thank Clarissa M. Spivakovsky for many enlightening discussions on tropospheric OH and CH_3CCl_3 lifetimes. We gratefully acknowledge Y. Kondo (Research Center for Advanced Science and Technology, University of Tokyo), Y. Zhao (University of Toronto), and M. Koike (Department of Earth and Planetary Science, Graduate School of Science, University of Tokyo) for CO column data measurements from Rikubetsu, Japan. The data from the Jungfraujoch have been derived by the group of the University of Liège, with funding primarily provided by the Office of Scientific, Technical and Cultural Affairs (OSTC), Brussels. J. A. Logan acknowledges the assistance of Chris Veldt with emissions factors in Europe and many useful discussions on CO emissions. This research was supported by the NASA ACMAP program and by the National Science Foundation, grants ATM-9320078, ATM-9903529, ATM-0236501 and ATM-0554804.

References

Allen, D. J., P. Kasibhatla, A. M. Thompson, R. B. Rood, B. G. Doddridge, K. E. Pickering, R. D. Hudson, and S.-J. Lin (1996a), Transport-induced interannual variability of carbon monoxide determined using a chemistry and transport model, *J. Geophys. Res.*, *101*, 28,655–28,669.

Allen, D. J., R. B. Rood, A. M. Thompson, and R. D. Hudson (1996b), Three-dimensional radon 222 calculations using assimilated meteorological data and a convective mixing algorithm, *J. Geophys. Res.*, *101*, 6871–6881.

Allen, D. J., K. E. Pickering, and A. Molod (1997), An evaluation of deep convective mixing in the Goddard Chemical Transport Model using International Satellite Cloud Climatology Project cloud parameters, *J. Geophys. Res.*, *102*, 25,467–25,476.

Allen, D., K. Pickering, and M. Fox-Rabinovitz (2004), Evaluation of pollutant outflow and CO sources during TRACE-P using model-calculated, aircraft-based, and Measurements of Pollution in the Troposphere (MOPITT)-derived CO concentrations, *J. Geophys. Res.*, *109*, D15S03, doi:10.1029/2003JD004250.

Altshuller, P. (1991), The production of carbon monoxide by the homogeneous NO_x-induced photooxidation of volatile organic compounds in the troposphere, *J. Atmos. Chem.*, *13*, 155–182.

Andreae, M., and P. Merlet (2001), Emission of trace gases and aerosols from biomass burning, *Global Biogeochem. Cycles*, *15*, 955–966.

Arakawa, A., and W. H. Schubert (1974), Interaction of cumulus cloud ensemble with the large-scale environment, Part I, *J. Atmos. Sci.*, *31*, 671–701.

Arellano, A. F., and P. G. Hess (2006), Sensitivity of top-down estimates of CO sources to GCTM transport, *Geophys. Res. Lett.*, *33*, L21807, doi:10.1029/2006GL027371.

Arellano, A. F., Jr., P. S. Kasibhatla, L. Giglio, G. R. van der Werf, and J. T. Randerson (2004), Correction to "Top-down estimates of global CO sources using MOPITT measurements", *Geophys. Res. Lett.*, *31*, L12108, doi:10.1029/2004GL020311.

Arellano, A. F., Jr., P. S. Kasibhatla, L. Giglio, G. R. van der Werf, J. T. Randerson, and G. J. Collatz (2006), Time-dependent inversion estimates of global biomass-burning CO emissions using Measurement of Pollution in the Troposphere (MOPITT) measurements, *J. Geophys. Res.*, *111*, D09303, doi:10.1029/2005JD006613.

Arino, O., and J.-M. Rosaz (1999), 1997 and 1998 World ATSR Fire Atlas using ERS-2 ATSR-2 data, in *Proceedings Joint Fire Science Conference*, pp. 177–182, Univ. of Idaho, Boise.

Bashmakov, I. (1992), Greenhouse gas emissions inventory of the former Soviet Union: Energy related emissions, 1988, Clim. Change Div., U. S. Environ. Prot. Agency, Washington, D. C.

Bates, T. S., K. C. Kelly, J. E. Johnson, and R. H. Gammon (1995), Regional and seasonal variations in the flux of oceanic carbon monoxide to the atmosphere, *J. Geophys. Res.*, *100*, 23,093–23,101.

Beaton, S. P., G. A. Bishop, and D. H. Stedman (1992), Emission characteristics of Mexico City vehicles, *J. Air Waste Manage. Assoc.*, *42*, 1424–1429.

Bekki, S., K. S. Law, and J. A. Pyle (1994), Effect of ozone depletion on atmospheric CH_4 and CO concentrations, *Nature*, *371*, 595–597.

Benkovitz, C. M., M. T. Scholtz, J. Pacyna, L. Tarrason, J. Dignon, E. C. Voldner, P. A. Spiro, J. A. Logan, and T. E. Graedel (1996), Global gridded inventories of anthropogenic emissions of sulfur and nitrogen, *J. Geophys. Res.*, *101*, 29,239–29,253.

Bergamaschi, P., R. Hein, M. Heimann, and P. J. Crutzen (2000a), Inverse modeling of the global CO cycle: 1. Inversion of CO mixing ratios, *J. Geophys. Res.*, *105*, 1909–1927.

Bergamaschi, P., R. Hein, C. A. M. Brenninkmeijer, and P. J. Crutzen (2000b), Inverse modeling of the global CO cycle: 2. Inversion of $^{13}C/^{12}C$ and $^{18}O/^{16}O$ isotope ratios, *J. Geophys. Res.*, *105*, 1929–1945.

Bethkenhagen, J., R. Melzer, C. Schwartau, and D. Cornelson (1988), SO_2 und NO_x emissionen in der DDR, *DIW Beitr. Strukt.*, *102*, Deutsches Inst. fur Wirtschaftsforschung, Berlin.

Bey, I., D. J. Jacob, R. M. Yantosca, J. A. Logan, B. D. Field, A. M. Fiore, Q. Li, H. Liu, L. J. Mickley, and M. Schultz (2001a), Global modeling of tropospheric chemistry with assimilated meteorology: Model description and evaluation, *J. Geophys. Res.*, *106*, 23,073–23,095.

Bey, I., D. J. Jacob, J. A. Logan, and R. M. Yantosca (2001b), Asian chemical outflow to the Pacific: Origins, pathways and budgets, *J. Geophys. Res.*, *106*, 23,097–23,113.

Bloom, S., et al. (2005), Documentation and validation of the Goddard Earth Observing System (GEOS) Data Assimilation System–Version 4, *Tech. Rep. Ser. Global Model. Data Assimilation 104606*, Global Model. Assimilation Off., Natl. Aeronaut. Space Admin., Greenbelt, Md.

Bouscaren, R. (1991), *Default Emissions Factors Handbook*, CORINAIR Inventory of the Commission of the European Community, CITEPA, Paris.

Bradley, K. S., D. H. Stedman, and G. A. Bishop (1999), A global inventory of carbon monoxide emissions from motor vehicles, *Chemosphere Global Change Sci.*, *1*, 65–72.

Bretterton, E. A., and M. R. Hoffmann (1988), Henry's law constants of some environmentally important aldehydes, *Environ. Sci. Technol.*, *22*, 1415–1418.

Brunke, E.-G., H. E. Scheel, and W. Seiler (1990), Trends of tropospheric CO, N_2O and CH_4 as observed at Cape Point, South Africa, *Atmos. Environ, Part A*, *24*, 585–595.

Butler, J. H., J. W. Elkins, T. M. Thompson, B. D. Hall, T. H. Swanson, and V. Koropalov (1991), Oceanic consumption of CH_3CCl_3: Implications for tropospheric OH, *J. Geophys. Res.*, *96*, 22,347–22,355.

Cahoon, D. R., B. J. Stocks, J. S. Levine, W. R. Coffer III, and J. M. Pierson (1994), Satellite analysis of the severe 1987 forest fires in northern China and southeastern Siberia, *J. Geophys. Res.*, *99*, 18,627–18,638.

Cape, J. N., J. Methven, and L. E. Hudson (2000), The use of trajectory cluster analysis to interpret trace gas measurements at Mace Head, Ireland, *Atmos. Environ.*, *34*, 3651–3663.

Carmichael, G. R., et al. (2003), Evaluating regional emission estimates using the TRACE-P observations, *J. Geophys. Res.*, *108*(D21), 8810, doi:10.1029/2002JD003116.

Chin, M., P. Ginoux, S. Kinne, O. Torres, B. Holben, B. Duncan, R. Martin, J. Logan, A. Higurashi, and T. Nakajima (2002), Tropospheric aerosol optical thickness from the GOCART model and comparisons with satellite and Sun photometer measurements, *J. Atmos. Sci.*, *59*, 461–483.

China Statistical Information and Consultancy Service Centre (1988), *China Statistical Yearbook*, Beijing.

Connors, V. S., B. B. Gormsen, S. Nolf, and H. G. Reichle Jr. (1999), Spaceborne observations of the global distribution of carbon monoxide in the middle troposphere during April and October 1994, *J. Geophys. Res.*, *104*, 21,455–21,470.

Conrad, R., W. Seiler, G. Bunse, and H. Giehl (1982), Carbon monoxide in seawater (Atlantic Ocean), *J. Geophys. Res.*, *87*, 8839–8852.

Crutzen, P. J. (1973), A discussion of the chemistry of some minor constituents in the stratosphere and troposphere, *Pure App. Geophys.*, *106–109*, 1385–1399.

Cullis, C. F., and M. M. Hirschler (1989), Man's emissions of carbon monoxide and hydrocarbons into the atmosphere, *Atmos. Environ.*, *23*, 1195–1203.

Daniel, J. S., and S. Solomon (1988), On the climate forcing of carbon monoxide, *J. Geophys. Res.*, *103*, 13,249–13,260.

Department of Transportation (1986), *Highway Statistics*, Federal Highway Admin., Washington, D. C.

Dickerson, R. R., M. O. Andreae, T. Campos, O. L. Mayol-Bracero, C. Neusuess, and D. G. Streets (2002), Analysis of black carbon and carbon monoxide observed over the Indian Ocean: Implications for emissions and photochemistry, *J. Geophys. Res.*, *107*(D19), 8017, doi:10.1029/2001JD000501.

Dlugokencky, E. J., E. G. Dutton, P. C. Novelli, P. P. Tans, K. A. Masarie, K. O. Lantz, and S. Madronich (1996), Changes in CH_4 and CO growth rates after the eruption of Mt. Pinatubo and their link with changes in tropical tropospheric UV flux, *Geophys. Res. Lett.*, *23*, 2761–2764.

Dlugokencky, E. J., K. A. Masarie, P. M. Lang, and P. P. Tans (1998), Continuing decline in the growth rate of the atmospheric methane burden, *Nature*, *393*, 447–450.

Duncan, B. N., and I. Bey (2004), A modeling study of the export pathways of pollution from Europe: Seasonal and interannual variations (1987–1997), *J. Geophys. Res.*, *109*, D08301, doi:10.1029/2003JD004079.

Duncan, B. N., D. Portman, I. Bey, and C. M. Spivakovsky (2000), Parameterization of OH for efficient computation in chemical tracer models, *J. Geophys. Res.*, *105*, 12,259–12,262.

Duncan, B. N., R. V. Martin, A. C. Staudt, R. Yevich, and J. A. Logan (2003a), Interannual and seasonal variability of biomass burning emissions constrained by satellite observations, *J. Geophys. Res.*, *108*(D2), 4100, doi:10.1029/2002JD002378.

Duncan, B. N., I. Bey, M. Chin, L. J. Mickley, T. D. Fairlie, R. V. Martin, and H. Matsueda (2003b), Indonesian wildfires of 1997: Impact on tropospheric chemistry, *J. Geophys. Res.*, *108*(D15), 4458, doi:10.1029/2002JD003195.

European Monitoring Environmental Programme (1997), Transboundary air pollution in Europe, Part 1: Emissions, dispersion, and trends of acidifying and eutrophying agents, *EMEP/MSC-W Report 1/97*, Norwegian Meteorol. Inst., Oslo.

Federal Highway Administration (2001), Traffic volume trends, U. S. Dep. of Transportation, Washington, D. C.

Fioletov, V. E., G. E. Bodeker, A. J. Miller, R. D. McPeters, and R. Stolarski (2002), Global and zonal total ozone variations estimated from ground-based and satellite measurements: 1964–2000, *J. Geophys. Res.*, *107*(D22), 4647, doi:10.1029/2001JD001350.

Fu, L., J. Hao, D. He, and K. He (2001), Assessment of vehicular pollution in China, *J. Air Waste Manage. Assoc.*, *51*, 658–668.

Galanter, M., H. Levy II, and G. R. Carmichael (2000), Impacts of biomass burning on tropospheric CO, NO_x, and O_3, *J. Geophys. Res.*, *105*, 6633–6653.

Granier, C., G. Pétron, J.-F. Müller, and G. Brasseur (2000), The impact of natural and anthropogenic hydrocarbons on the tropospheric budget of carbon monoxide, *Atmos. Environ.*, *34*, 5255–5270.

Gregory, G. L., et al. (1999), Chemical characteristics of Pacific tropospheric air in the region of the Intertropical Convergence Zone and South Pacific Convergence Zone, *J. Geophys. Res.*, *104*, 5677–5696.

Guenther, A., et al. (1995), A global model of natural volatile organic compound emissions, *J. Geophys. Res.*, *100*, 8873–8892.

Hao, W. M., and M.-H. Liu (1994), Spatial and temporal distribution of tropical biomass burning, *Global Biogeochem. Cycles*, *8*, 495–503.

Hatakeyama, S., K. Izumi, T. Fukuyama, H. Akimoto, and N. Washida (1991), Reactions of OH with alpha-pinene and beta-pinene in air: Estimate of global CO production from the atmospheric oxidation of terpenes, *J. Geophys. Res.*, *96*, 947–958.

Herman, J. R., P. K. Bhartia, O. Torres, C. Hsu, C. Seftor, and E. Celarier (1997), Global distribution of UV-absorbing aerosols from Nimbus 7/TOMS data, *J. Geophys. Res.*, *102*, 16,911–16,922.

Herman, J. R., N. Krotkov, E. Celarier, D. Larko, and G. Labow (1999), Distribution of UV radiation at the Earth's surface from TOMS-measured UV-backscattered radiances, *J. Geophys. Res.*, *104*, 12,059–12,076.

Holloway, T., H. Levy II, and P. Kasibhatla (2000), Global distribution of carbon monoxide, *J. Geophys. Res.*, *105*, 12,123–12,147.

Intergovernmental Panel on Climate Change (1996), *Climate Change 1995: The Science of Climate Change*, edited by J. T. Houghton et al., 584 pp., Cambridge Univ. Press, New York.

International Iron and Steel Institute (1987), *Steel Statistical Yearbook 1987*, Int. Iron and Steel Inst., Brussels, Belgium.

Jacob, D. J. (2000), Heterogeneous chemistry and tropospheric ozone, *Atmos. Environ.*, *34*, 2131–2159.

Jacob, D. J., B. D. Field, E. M. Jin, I. Bey, Q. Li, J. A. Logan, R. M. Yantosca, and H. B. Singh (2002), Atmospheric budget of acetone, *J. Geophys. Res.*, *107*(D10), 4100, doi:10.1029/2001JD000694.

Jaffe, L. S. (1973), Carbon monoxide in the biosphere–Sources, distribution, and concentrations, *J. Geophys. Res.*, *78*, 5293–5305.

Kanakidou, M., and P. J. Crutzen (1999), The photochemical source of carbon monoxide: Importance, uncertainties and feedbacks, *Chemosphere Global Change Sci.*, *1*, 91–109.

Kanakidou, M., et al. (1999), 3-D global simulations of tropospheric CO distributions–Results of the GIM/IGAC intercomparison 1997 exercise, *Chemosphere Global Change Sci.*, *1*, 263–282.

Karlsdóttir, S., I. S. A. Isaksen, and G. Myhre (2000), Trend analysis of O_3 and CO in the period 1980–1996: A three-dimensional model study, *J. Geophys. Res.*, *105*, 28,907–28,933.

Kasibhatla, P., A. Arellano, J. A. Logan, P. I. Palmer, and P. Novelli (2002), Top-down estimate of a large source of atmospheric carbon monoxide associated with fuel combustion in Asia, *Geophys. Res. Lett.*, *29*(19), 1900, doi:10.1029/2002GL015581.

Kasischke, E. S., E. J. Hyer, P. C. Novelli, L. P. Bruhwiler, N. H. F. French, A. I. Sukhinin, J. H. Hewson, and B. J. Stocks (2005), Influences of boreal fire emissions on Northern Hemisphere atmospheric carbon and carbon monoxide, *Global Biogeochem. Cycles*, *19*, GB1012, doi:10.1029/2004GB002300.

Khalil, M. A. K., and R. A. Rasmussen (1994), Global decrease in atmospheric carbon monoxide concentration, *Nature*, *370*, 639–641.

Kleinman, L. I. (1994), Low and high NO_x tropospheric chemistry, *J. Geophys. Res.*, *99*, 16,831–16,838.

Lelieveld, J., et al. (2001), The Indian Ocean Experiment: Widespread air pollution from South and Southeast Asia, *Science*, *291*, 1031–1036.

Levine, J. S. (1999), The 1997 fires in Kalimantan and Sumatra, Indonesia: Gaseous and particulate emissions, *Geophys. Res. Lett.*, *26*(7), 815–818.

Levy, H., II (1971), Normal atmosphere: Large radical and formaldehyde concentrations predicted, *Science*, *173*, 141–143.

Lin, S.-J., and R. B. Rood (1996), Multidimensional flux-form semi-Lagrangian transport schemes, *Mon. Weather Rev.*, *124*, 2046–2070.

Lind, J. A., and G. L. Kok (1986), Henry's law determinations for aqueous solutions of hydrogen peroxide, methylhydroperoxide, and peroxyacetic acid, *J. Geophys. Res.*, *91*, 7889–7895.

Linnenbom, V. J., J. W. Swinnerton, and R. A. Lamontagne (1973), The ocean as a source for atmospheric carbon monoxide, *J. Geophys. Res.*, *78*, 5333–5340.

Liu, H., D. J. Jacob, I. Bey, and R. M. Yantosca (2001), Constraints from ^{210}Pb and ^{7}Be on wet deposition and transport in a global three-dimensional chemical tracer model driven by assimilated meteorological fields, *J. Geophys. Res.*, *106*, 12,109–12,128.

Lobert, J., W. Keen, J. Logan, and R. Yevich (1999), Global chlorine emissions from biomass burning: Reactive chlorine emissions inventory, *J. Geophys. Res.*, *104*, 8373–8389.

Logan, J. A. (1999a), An analysis of ozonesonde data for the troposphere: Recommendations for testing 3-D models, and development of a gridded climatology for tropospheric ozone, *J. Geophys. Res.*, *104*, 16,115–16,149.

Logan, J. A. (1999b), An analysis of ozonesonde data for the lower stratosphere: Recommendations for testing models, *J. Geophys. Res.*, *104*, 16,151–16,170.

Logan, J. A., M. J. Prather, S. C. Wofsy, and M. B. McElroy (1981), Tropospheric chemistry: A global perspective, *J. Geophys. Res.*, *86*, 7210–7254.

Magi, L., F. Schweitzer, C. Pallares, S. Cherif, P. Mirabel, and C. George (1997), Investigation of the uptake rate for ozone and methyl hydroperoxide by water surfaces, *J. Phys. Chem. A*, *101*, 4943–4949.

Mahieu, E., R. Zander, L. Delbouille, P. Demoulin, G. Roland, and C. Servais (1997), Observed trends in total vertical column abundances of atmospheric gases from IR solar spectra recorded at the Jungfraujoch, *J. Atmos. Chem.*, *28*, 227–243.

Manning, M. R., C. A. M. Brenninkmeijer, and W. Allan (1997), Atmospheric carbon monoxide budget of the southern hemisphere: Implications of $^{13}C/^{12}C$ measurements, *J. Geophys. Res.*, *102*, 10,673–10,682.

Mari, C., D. J. Jacob, and P. Bechtold (2000), Transport and scavenging of soluble gases in a deep convective cloud, *J. Geophys. Res.*, *105*, 22,255–22,267.

Marland, G., T. A. Boden, R. J. Andres, A. L. Brenkert, and C. A. Johnston (1999), Global, regional, and national fossil fuel CO_2 emissions, in *Trends: A Compendium of Data on Global Change*, Carbon Dioxide Inf. Anal. Cent., Oak Ridge Natl. Lab., Oak Ridge, Tenn.

Martin, R. V., D. J. Jacob, R. M. Yantosca, M. Chin, and P. Ginoux (2003), Global and regional decreases in tropospheric oxidants from photochemical effects of aerosols, *J. Geophys. Res.*, *108*(D3), 4097, doi:10.1029/2002JD002622.

Merrill, J. T. (1989), Atmospheric long-range transport to the Pacific Ocean, in *Chemical Oceanography*, vol. 10, edited by R. A. Duce, et al., pp. 15–50, Elsevier, New York.

Mickley, L. J., P. P. Murti, D. J. Jacob, J. A. Logan, D. Rind, and D. Koch (1999), Radiative forcing from tropospheric ozone calculated with a unified chemistry-climate model, *J. Geophys. Res.*, *104*, 30,153–30,172.

Miyoshi, A., S. Hatakeyama, and N. Washida (1994), OH radical-initiated photooxidation of isoprene: An estimate of global CO production, *J. Geophys. Res.*, *99*, 18,779–18,787.

Molod, A., H. M. Helfand, and L. L. Takacs (1996), The climatology of parameterized physical processes in the GEOS-1 GCM and their impact on the GEOS-1 data assimilation system, *J. Clim.*, *9*, 764–785.

Moorthi, S., and M. J. Suarez (1992), Relaxed Arakawa-Schubert: A parameterization of moist convection for general circulation models, *Mon. Weather Rev.*, *120*, 979–1002.

Müller, J.-F., and T. Stavrakou (2005), Inversion of CO and NO_x emissions using the adjoint of the IMAGES model, *Atmos. Chem. Phys.*, *5*, 1157–1186.

National Bureau of Statistics of China (1998), *China Statistical Yearbook*, Beijing.

Novelli, P. C., L. P. Steele, and P. P. Tans (1992), Mixing ratios of carbon monoxide in the troposphere, *J. Geophys. Res.*, *102*, 12,855–12,861.

Novelli, P. C., K. A. Masarie, P. P. Tans, and P. M. Lang (1994), Recent changes in atmospheric carbon monoxide, *Science*, *263*, 1587–1590.

Novelli, P. C., K. A. Masarie, and P. M. Lang (1998), Distributions and recent changes in carbon monoxide in the lower troposphere, *J. Geophys. Res.*, *103*, 19,015–19,033.

Novelli, P. C., P. M. Lang, K. A. Masarie, D. F. Hurst, R. Myers, and J. W. Elkins (1999), Molecular hydrogen in the troposphere: Global distribution and budget, *J. Geophys. Res.*, *104*, 30,427–30,444.

Novelli, P. C., K. A. Masarie, P. M. Lang, B. D. Hall, R. C. Myers, and J. W. Elkins (2003), Reanalysis of tropospheric CO trends: Effects of the 1997–1998 wildfires, *J. Geophys. Res.*, *108*(D15), 4464, doi:10.1029/2002JD003031.

Olivier, J. G. J., A. F. Bouwman, C. W. M. van der Maas, J. J. M. Berdowski, C. Veldt, J. P. J. Bloos, A. J. H. Visschedijk, P. Y. J. Zandveld, and J. L. Haverlag (1996), Description of EDGAR version 2.0: A set of global emission inventories of greenhouse gases and ozone-depleting substances for all anthropogenic and most natural sources on a per country basis and on $1^\circ \times 1^\circ$ grid, 141 pp., *RIVM-Rep. 771060*, Natl. Inst. of Public Health and the Environ., Bilthoven, The Netherlands.

Olivier, J. G. J., J. Pieter, J. Bloos, J. J. M. Berdowski, A. J. H. Visschedijk, and A. F. Bouwman (1999), A 1990 global emission inventory of anthropogenic sources of carbon monoxide on $1^\circ \times 1^\circ$ developed in the framework of EDGAR/GEIA, *Chemosphere Global Change Sci.*, *1*, 1–17.

Olivier, J. G. J., J. J. M. Berdowski, J. A. H. W. Peters, J. Bakker, A. J. H. Visschedijk, and J.-P. J. Bloos (2001), Applications of EDGAR. Including a description of EDGAR 3.0: Reference database with trend data for 1970–1995, *RIVM Rep. no. 773301 001*, Natl. Inst. of Public Health and the Environ., Bilthoven, The Netherlands.

Organization for Economic Cooperative Development (1990), World Energy Statistics and Balances, 1985–1988, Int. Energ. Agency, Paris.

Organization for Economic Cooperative Development (1991a), Energy Statistics of OECD Countries 1980–89, Int. Energ. Agency, Paris.

Organization for Economic Cooperative Development (1991b), Energy Balances of OECD Countries 1980–1989, Int. Energ. Agency, Paris.

Orlando, J., B. Noziere, G. Tyndall, G. Orzechowska, S. Paulson, and Y. Rudich (2000), Product studies of the OH- and ozone-initiated oxidation of some monoterpenes, *J. Geophys. Res.*, *105*, 11,561–11,572.

Palmer, P. I., D. J. Jacob, A. M. Fiore, R. V. Martin, K. Chance, and T. P. Kurosu (2003), Mapping isoprene emissions over North America using formaldehyde column observations from space, *J. Geophys. Res.*, *108*(D6), 4180, doi:10.1029/2002JD002153.

Paulson, S. E., and J. H. Seinfeld (1992), Development and evaluation of a photooxidation mechanism for isoprene, *J. Geophys. Res.*, *97*, 20,703–20,715.

Pétron, G., C. Granier, B. Khattatov, J. Lamarque, V. Yudin, J. Müller, and J. Gille (2002), Inverse modeling of carbon monoxide surface emissions using Climate Monitoring and Diagnostics Laboratory network observations, *J. Geophys. Res.*, *107*(D24), 4761, doi:10.1029/2001JD001305.

Pétron, G., C. Granier, B. Khattatov, V. Yudin, J.-F. Lamarque, L. Emmons, J. Gille, and D. P. Edwards (2004), Monthly CO surface sources inventory based on the 2000–2001 MOPITT satellite data, *Geophys. Res. Lett.*, *31*, L21107, doi:10.1029/2004GL020560.

Piccot, S., J. Watson, and J. Jones (1992), A global inventory of volatile organic compound emissions from anthropogenic sources, *J. Geophys. Res.*, *97*, 9897–9912.

Pickering, K. E., et al. (1996), Convective transport of biomass burning emissions over Brazil during TRACE A, *J. Geophys. Res.*, *101*, 23,993–24,012.

Prinn, R. G., et al. (2005), Evidence for variability of atmospheric hydroxyl radicals over the past quarter century, *Geophys. Res. Lett.*, *32*, L07809, doi:10.1029/2004GL022228.

Reichle, H. G., Jr., et al. (1999), Space shuttle based global CO measurements during April and October 1994, MAPS instrument, data reduction, and data validation, *J. Geophys. Res.*, *104*, 21,443–21,454.

Reissell, A., C. Harry, S. Aschmann, R. Atkinson, and J. Arey (1999), Formation of acetone from the OH radical- and O_3-initiated reactions of a series of monoterpenes, *J. Geophys. Res.*, *104*, 13,869–13,879.

Rinsland, C. P., et al. (1998), Northern and southern hemisphere ground-based infrared spectroscopic measurements of tropospheric carbon monoxide and ethane, *J. Geophys. Res.*, *103*, 28,197–28,217.

Rinsland, C. P., et al. (1999), Infrared solar spectroscopic measurements of free tropospheric CO, C_2H_6, and HCN above Mauna Loa, Hawaii: Seasonal variations and evidence for enhanced emissions from the Southeast Asian tropical fires of 1997–1998, *J. Geophys. Res.*, *104*, 18,667–18,680.

Rinsland, C. P., E. Mahieu, R. Zander, P. Demoulin, J. Forrer, and B. Buchmann (2000), Free tropospheric CO, C_2H_6, and HCN above central Europe: Recent measurements from the Jungfraujoch station including the detection of elevated columns during 1998, *J. Geophys. Res.*, *105*, 24,235–24,249.

Samaras, Z., and K.-H. Zierock (1989), Summary report of the CORINAIR Working Group on Emission factors for Calculating 1985 Emissions from Road traffic, vol. 3, 38 pp., Comm. of Eur. Commun., Luxembourg.

Sander, S. P., et al. (2003), Chemical kinetics and photochemical data for use in atmospheric studies, *Eval. 14*, Jet Propul. Lab., Natl. Aeronaut. and Space Admin., Greenbelt, Md.

Sanhueza, E., Y. Dong, D. Scharffe, J. M. Lobert, and P. J. Crutzen (1998), Carbon monoxide uptake by temperate forest soils: The effects of leaves and humus layers, *Tellus, Ser. B*, *50*, 51–58.

Sawyer, R. F., R. A. Harley, S. H. Cadle, J. M. Norbeck, R. Slott, and H. A. Bravo (2000), Mobile sources critical review: 1998 NARSTO assessment, *Atmos. Environ.*, *34*, 2161–2181.

Schneider, H. R., D. B. A. Jones, M. B. McElroy, and G. Shi (2000), Analysis of residual mean transport in the stratosphere: 1. Model description and comparison with satellite data, *J. Geophys. Res.*, *105*(D15), 19,991–20,012.

Schubert, S. D., R. B. Rood, and J. Pfaendtner (1993), An assimilated data set for earth science applications, *Bull. Am. Meteorol. Soc.*, *74*, 2331–2342.

Schubert, S. D., et al. (1995), A multiyear assimilation with the GEOS-1 system: Overview and results, *Tech. Memo. 104606*, vol. 6, 207 pp., Goddard Space Flight Cent., Greenbelt, Md.

Seiler, W. (1974), The cycle of atmospheric CO, *Tellus*, *27*, 116–135.

Seiler, W., and U. Schmidt (1974), Dissolved nonconservative gases in seawater, in *The Sea*, vol. 5, edited by. E. P. Goldberg, pp. 219–243, John Wiley, Hoboken, N. J.

Shindell, D. T., et al. (2006), Multimodel simulations of carbon monoxide: Comparison with observations and projected near-future changes, *J. Geophys. Res.*, *111*, D19306, doi:10.1029/2006JD007100.

Simmonds, P. G., S. Seuring, G. Nickless, and R. G. Derwent (1997), Segregation and interpretation of ozone and carbon monoxide measurements by air mass origin at the TOR station Mace Head, Ireland from 1987 to 1995, *J. Atmos. Chem.*, *28*, 45–49.

Singh, H., et al. (2000), Distribution and fate of selected oxygenated organic species in the troposphere and lower stratosphere over the Atlantic, *J. Geophys. Res.*, *105*, 3795–3805.

Sinton, J. E. (2001), Accuracy and reliability of China's energy statistics, *China Econ. Rev.*, *12*(4), 373–383.

Sinton, J. E., and D. G. Fridley (2000), What goes up: Recent trends in China's energy consumption, *Energ. Policy*, *28*, 671–687.

Spivakovsky, C. M., et al. (2000), Three-dimensional climatological distribution of tropospheric OH: Update and evaluation, *J. Geophys. Res.*, *105*, 8931–8980.

Streets, D. G., and S. T. Waldhoff (2000), Present and future emissions of air pollutants in China: SO_2, NO_x, and CO, *Atmos. Environ.*, *34*, 363–374.

Streets, D. G., K. Jiang, X. Hu, J. E. Sinton, X. Zhang, D. Xu, M. Z. Jacobson, and J. E. Hansen (2001), Recent reductions in China's greenhouse gas emissions, *Science*, *294*, 1835–1837.

Streets, D. G., et al. (2003), An inventory of gaseous and primary aerosol emissions in Asia in the year 2000, *J. Geophys. Res.*, *108*(D21), 8809, doi:10.1029/2002JD003093.

Streets, D. G., Q. Zhang, L. Wang, K. He, J. Hao, Y. Wu, Y. Tang, and G. R. Carmichael (2006), Revisiting China's CO emissions after the Transport and Chemical Evolution over the Pacific (TRACE-P) mission: Synthesis of inventories, atmospheric modeling, and observations, *J. Geophys. Res.*, *111*, D14306, doi:10.1029/2006JD007118.

Stump, F., S. Tejada, W. Ray, D. Dropkin, and F. Black (1989), The influence of ambient temperatures on tailpipe emissions from 1984–1987 model year light-duty gasoline motor vehicles, *Atmos. Environ.*, *23*, 307–320.

Takacs, L. L. (1995), Documentation of the ARIES/GEOS Dynamical Core: Version 2, *NASA-TM-104606-vol. 5*, Goddard Space Flight Cent., Natl. Aeronaut. and Space Admin., Greenbelt, Md.

Takacs, L. L., A. Molod, and T. Wang (1994), Documentation of the Goddard Earth Observing System (GEOS) General Circulation Model–Version 1, *NASA-TM-104606-vol. 1*, Goddard Space Flight Cent., Natl. Aeronaut. and Space Admin., Greenbelt, Md.

Talbot, R. W., et al. (1996), Chemical characteristics of continental outflow over the tropical South Atlantic Ocean from Brazil and Africa, *J. Geophys. Res.*, *101*, 24,187–24,202.

Tie, X., C.-Y. J. Kao, and E. J. Mroz (1992), Net yield of OH, CO, and O_3, from the oxidation of atmospheric methane, *Atmos. Environ., Part A*, *26*, 125–136.

Torres, O., P. K. Bhartia, J. R. Herman, Z. Ahmad, and J. Gleason (1998), Derivation of aerosol properties from satellite measurements of backscattered ultraviolet radiation: Theoretical basis, *J. Geophys. Res.*, *103*, 17,099–17,110.

United Nations (1991), *Industrial Statistics Yearbook*, Dep. of Economic and Social Affairs, Statistical Office, U. N., New York.

United Nations (1998), *1996 Energy Statistics Yearbook*, Dep. of Economic and Social Inf. and Policy Anal., Statistics Div., U. N., New York.

U.S. Bureau of Mines (1987), *Mineral Yearbook: Iron and Steel Scrap*, U. S. Dept. of the Interior, Washington D. C.

U.S. Environmental Protection Agency (1985), Compilation of Air Pollution Emission Factors, *Publ. AP-42*, Washington, D. C.

U.S. Environmental Protection Agency (1989), The 1985 NAPAP emissions inventory (Version 2): Development of the annual data and modelers' tapes, *Report EPA/600/7-89/012a*, Research Triangle Park, N. C.

U.S. Environmental Protection Agency (1991), National air pollutant emission estimates, 1940–1990, *EPA-450/4-91-026*, Research Triangle Park, N. C.

U.S. Environmental Protection Agency (1992), National air pollutant emissions estimates, 1900–1991, *EPA-454/R-92-013*, Research Triangle Park, N. C.

U.S. Environmental Protection Agency (1993), Supplement F to Compliation of air pollutant emission factors, vol. 1, Stationary and point sources, *Rep. AP-42*, Research Triangle Park, N. C.

U.S. Environmental Protection Agency (1994), National air pollutant emissions trends, 1900–1993, *EPA-454/R-94-027*, Research Triangle Park, N. C.

U.S. Environmental Protection Agency (1997), National air pollutant emission trends, 1990–1996, *EPA-454/R-97-011*, Research Triangle Park, N. C.

U.S. Environmental Protection Agency (2000), National air pollutants emission trends report, 1900–1998, *EPA-454/R-00-002*, Off. of Air Quality and Stand., Research Triangle Park, N. C. (Available at http://www.epa.gov/ttn/chief/publications.html)

van Aardenne, J. A., G. R. Carmichael, H. Levy II, D. Streets, and L. Hordijk (1999), Anthropogenic NO_x emissions in Asia in the period 1990–2020, *Atmos. Environ.*, *33*, 633–646.

Veldt, C. (1991), Emissions of SO_2, NO_x, VOC, and CO from East European countries, *Atmos. Environ, Part A*, *25*, 2683–2700.

Vestreng, V., and E. Storen (2000), Analysis of UNECE/EMEP emission data MSC-W status report 2000, *EMEP MSC-W Note 1/00*, Norwegian Meteorol. Inst., Blindern, Norway.

Vinckier, C., F. Compernolle, A. M. Saleh, N. Vanoof, and I. Vanhees (1998), Product yields of the alpha-pinene reaction with hydroxyl radicals and the implication on the global emission of trace compounds in the atmosphere, *Fresenius Environ. Bull.*, *7*(5–6), 361–368.

Volk, C. M., J. W. Elkins, D. W. Fahey, G. S. Dutton, J. M. Gilligan, M. Loewenstein, J. R. Podolske, K. R. Chan, and M. R. Gunson (1997), Evaluation of source gas lifetimes from stratospheric observations, *J. Geophys. Res.*, *102*, 25,543–25,564.

Wang, J. S., J. A. Logan, M. B. McElroy, B. N. Duncan, I. A. Megretskaia, and R. M. Yantosca (2004), A 3-D model analysis of the slowdown and interannual variability in the methane growth rate from 1988 to 1997, *Global Biogeochem. Cycles*, *18*, GB3011, doi:10.1029/2003GB002180.

Wang, X., D. L. Mauzerall, Y. Hu, A. G. Russell, E. D. Larson, J. H. Woo, D. G. Streets, and A. Guenther (2005), A high-resolution emission inventory for eastern China in 2 000 and three scenarios for 2020, *Atmos. Environ.*, *39*, 5917–5933.

Wang, Y., D. J. Jacob, and J. A. Logan (1998), Global simulation of tropospheric O_3-NO_x-hydrocarbon chemistry: 1. Model formulation, *J. Geophys. Res.*, *103*, 10,713–10,725.

Welzel, K., and P. Davids (1978), *Die Kohlenmonoxidemissionen in der Dundesrepublik Deutschland in den Jahren 1965,1970,1974 und 1974 ind im Lande Nordrhein-Westralen in den Jahren 1973 und 1974*, Kohlhammer, Stuttgart, Germany.

Wild, O., J. K. Sundet, M. J. Prather, I. S. A. Isaksen, H. Akimoto, E. V. Browell, and S. J. Oltmans (2003), Chemical transport model ozone simulations for spring 2001 over the western Pacific: Comparisons with TRACE-P lidar, ozonesondes, and Total Ozone Mapping Spectrometer columns, *J. Geophys. Res.*, *108*(D21), 8826, doi:10.1029/2002JD003283.

World Bank (1985), China: The energy sector, Annex 3 to *China: Long term Development Issues and Options*, World Bank, Washington, D. C.

World Meteorological Organization (1999), Scientific assessment of ozone depletion: 1998, *WMO*, *Rep. 44*, Global Ozone Res. Monit. Proj., World Meteorol. Org., Geneva.

Wotawa, G., P. Novelli, M. Trainer, and C. Granier (2001), Inter-annual variability of average summertime CO concentrations in the northern hemisphere explained by boreal forest fires in North America and Russia, *Geophys. Res. Lett.*, *28*, 4575–4578.

Yevich, R., and J. A. Logan (2003), An assessment of biofuel use and burning of agricultural waste in the developing world, *Global Biogeochem. Cycles*, *17*(4), 1095, doi:10.1029/2002GB001952.

Yung, Y. L., C. Shia, and R. L. Herman (1999), Is the biomass burning source of CO decreasing?, *Chemosphere Global Change Sci.*, *1*, 83–90.

Yurganov, L. N., et al. (2004), A quantitative assessment of the 1998 carbon monoxide emission anomaly in the Northern Hemisphere based on total column and surface concentration measurements, *J. Geophys. Res.*, *109*, D15305, doi:10.1029/2004JD004559.

Yurganov, L. N., et al. (2005), Increased northern hemispheric carbon monoxide burden in the troposphere in 2002 and 2003 detected from the ground and from space, *Atmos. Chem. Phys. Disc.*, *4*, 4999–5017.

Zander, R., P. Demoulin, D. H. Ehhalt, U. Schmidt, and C. P. Rinsland (1989), Secular increase of the total vertical column abundance of carbon monoxide above central Europe since 1950, *J. Geophys. Res.*, *94*, 11,021–11,028.

Zhang, J., K. R. Smith, R. Uma, Y. Ma, V. V. N. Kishore, K. Lata, M. A. K. Khalil, R. A. Rasmussen, and S. T. Thornloe (1999), Carbon monoxide from cookstoves in developing countries: 1 Emissions factors, *Chemosphere Global Change Sci.*, *1*, 353–366.

Zhang, J., K. R. Smith, Y. Ma, S. Ye, F. Jiang, W. Qi, P. Liu, M. A. K. Khalil, R. A. Rasmussen, and S. T. Thornloe (2000), Greenhouse gases and other airborne pollutants from household stoves in China: A database for emission factors, *Atmos. Environ.*, *34*, 4537–4549.

Zhao, Y., Y. Kondo, F. J. Murcray, X. Liu, M. Koike, K. Kita, H. Nakajima, I. Murata, and K. Suzuki (1997), Carbon monoxide column abundances and tropospheric concentrations retrieved from high resolution ground-based infrared solar spectra at 43.5°N over Japan, *J. Geophys. Res.*, *102*, 23,403–23,411.

Zhao, Y., Y. Kondo, F. J. Murcray, X. Liu, M. Koike, H. Irie, K. Strong, K. Suzuki, M. Sera, and Y. Ikegami (2000), Seasonal variations of HCN over northern Japan measured by ground-based infrared solar spectroscopy, *Geophys. Res. Lett.*, *27*, 2085–2088.

Zimmerman, P. R., R. B. Chatfield, J. Fishman, P. J. Crutzen, and P. L. Hanst (1978), Estimates on the production of CO and H_2 from the oxidation of hydrocarbon emissions from vegetation, *Geophys. Res. Lett.*, *5*, 679–682.

I. Bey, Laboratoire de Modélisation de Chimie Atmosphérique, École Polytechnique Fédérale de Lausanne, CH-1015 Lausanne, Switzerland.

B. N. Duncan, Goddard Earth Sciences and Technology Center, University of Maryland, Baltimore County, Baltimore, MD 21250, USA. (bryan.n.duncan@nasa.gov)

N. B. Jones, Department of Chemistry, University of Wollongong, Wollongong, NSW 2522, Australia.

J. A. Logan, I. A. Megretskaia, and R. M. Yantosca, School of Engineering and Applied Sciences, Harvard University, Cambridge, MA 02138, USA.

P. C. Novelli, Global Monitoring Division, Earth System Research Laboratory, NOAA, Boulder, CO 80305, USA.

C. P. Rinsland, NASA Langley Research Center, Hampton, VA 23681, USA.